2010

Block of mouse Slo1 and Slo3 K+ channels by CTX, IbTX, TEA, 4-AP and quinidine

Qiong-Yao Tang
Washington University School of Medicine in St. Louis

Zhe Zhang
Washington University School of Medicine in St. Louis

Xiao-Ming Xia
Washington University School of Medicine in St. Louis

Christopher J. Lingle
Washington University School of Medicine in St. Louis

Block of mouse Slo1 and Slo3 K⁺ channels by CTX, IbTX, TEA, 4-AP and quinidine

Qiong-Yao Tang,[†] Zhe Zhang,[†] Xiao-Ming Xia and Christopher J. Lingle*

Department of Anesthesiology; Washington University School of Medicine; St. Louis, MO USA

[†]Current address: Department of Physiology and Biophysics; Virginia Commonwealth University; School of Medicine; Richmond, VA USA

pH-regulated Slo3 channels, perhaps exclusively expressed in mammalian sperm, may play a role in alkalization-mediated K⁺ fluxes associated with sperm capacitation. The Slo3 channel shares extensive homology with Ca^{2+}- and voltage-regulated BK-type Slo1 K⁺ channels. Here, using heterologous expression in oocytes, we define distinctive differences in pharmacological properties of Slo3 and Slo1 currents, examine blockade in terms of distinct blocking models, and, for some blockers, use mutated constructs to evaluate determinants of block. Slo3 is resistant to block by the standard Slo1 blockers, iberiotoxin, charybdotoxin and extracellular TEA. Slo3 is relatively insensitive to extracellular 4-AP up to 100 mM, while Slo1 is blocked in a voltage-dependent fashion consistent with block on the extracellular side of the channel. Block of both Slo1 and Slo3 by cytosolic 4-AP can be described by open channel block, with Slo3 being ~10–15-fold more sensitive, but exhibiting weaker voltage-dependence of block. The cytosolic concentrations of 4-AP required to block Slo3 make it unlikely that the effects of 4-AP on volume regulation in mammalian sperm is mediated by Slo3. Quinidine was more effective in blocking Slo3 than Slo1. For Slo1, quinidine block was favored by depolarization, irrespective of the side of application. For Slo3, quinidine block was relieved by depolarization, irrespective of the side of application, with strong block by less than 10 μM quinidine at potentials near 0 mV. The unusual voltage-dependence of block of Slo3 by quinidine may result from preferential binding of quinidine to closed Slo3 channels. The quinidine concentrations effective in blocking Slo3 suggest, that in experiments that have examined quinidine effects on sperm, any Slo3 currents would be almost completely inhibited.

Introduction

The pH-regulated Slo3 channel is a candidate for a mammalian sperm K⁺ channel[1] that may be activated during the robust elevations in pH that are an integral part of sperm hyperactivation, an essential step in the ability of sperm to fertilize ova.[2,3] Recent work has described a pH-sensitive K⁺ current, named KSper, in native mouse spermatocytes that is a candidate for a current mediated by Slo3,[4] but there are differences between the pH-sensitive current in spermatocytes and the properties of heterologously expressed Slo3 currents.[5,6] In particular, the current in spermatocytes appears to be relatively more strongly activated at more negative potentials and lower pH.[4] Furthermore, there may be kinetic differences between the two currents. Despite the apparent differences, Slo3 remains the best candidate as the molecular substrate of the KSper current. As yet, pharmacological tools that might prove useful for distinguishing a Slo3 current from other K⁺ channels in spermatocytes have not been defined.

Here, we undertake a pharmacological examination of Slo3 currents with the idea of identifying compounds that either through mechanism or concentration of action might prove useful for testing the molecular identity of the KSper current.[4] A challenge to such an endeavor is that, except for fortuitous identification of toxins, most compounds found to block a given K⁺ channel may also block a number of other K⁺ channels. However, despite promiscuity in blocking action by many K⁺ channel compounds, if the blocking affinity or other hallmarks of block are carefully identified, some compounds may still be of use for purposes of identification of a current in a native cell. In order to accomplish this, ideally one would like to know the true binding affinity of a blocking molecule to the particular channel state(s) to which the blocker binds. The challenge, of course, is how to obtain such estimates. Such estimates require not only measurements of blockade by a compound at multiple concentrations and voltages, but they also require knowledge about the correct molecular blocking model and the channel activation probability, which are often not known with certainty. For example,

fractional block of a current by an open channel blocker depends critically on the fractional activation of the target channel. Thus, the apparent effectiveness of block for most channel blockers depends not only on blocker concentration, but also on membrane voltage and channel open probability.

Here, in examining Slo3 pharmacology, we examine blocking effects over a range of blocker concentrations and voltages, while taking advantage of information about the fractional activation of Slo3 current.[5,6] We also compare Slo3 pharmacological sensitivity to that of its closely related homologue, the Ca^{2+}- and voltage-activated Slo1 (or BK-type) K^+ channel. We focus primarily on two categories of compounds: first, well-known blockers of Slo1 channels such as TEA[7] and scorpion toxins[8,9] and, second, general K^+ channel blockers that have previously been reported to have effects on spermatocyte function, namely 4-AP and quinine/quinidine.[10,11] For both Slo1 and Slo3, reasonable mechanistic frameworks are available that describe activation of conductance as a function of voltage and ligand. In conjunction with an examination of blocker action over a range of voltages and concentrations, it is then possible to make inferences regarding the molecular mechanism of blocker action. In such cases, estimates of blocker binding affinity can be made, or, if there remains uncertainty about the blocking mechanism, at least reasonable estimates of blocking effectiveness can be obtained. Since Slo1 and Slo3 share extensive amino acid identity, particularly through the pore domain,[1] any differences in sensitivity to block between these channels will facilitate definition of the blocking sites. Using this approach, the results show that Slo1 and Slo3 have remarkably distinct pharmacological sensitivities. Confirming earlier results from others[12] we identify the unique determinants in Slo1 that make it, but not Slo3, sensitive to extracellular scorpion toxins and TEA. Slo3 is ~25-fold more sensitive to cytosolic TEA than Slo1. Extracellular 4-AP blocks Slo1 channels with minimal effects on Slo3, while cytosolic 4-AP is more effective on Slo3 than on Slo1. Irrespective of the side of application, quinidine is relatively efficacious against Slo3 over Slo1. Analysis of the voltage- and concentration-dependence of Slo3 block by quinidine suggests that quinidine, whether accessing the Slo3 channel from the extracellular or cytosolic side of the membrane, reaches a binding site that may selectively stabilize the closed state of the channel. The unique characteristics of block of Slo3 by quinidine may prove of value in testing whether Slo3 underlies the KSper current.

Results

For routine examination of the pharmacological sensitivity of channels with a Slo3 pore domain, we have primarily used a construct termed MC13 (see Methods for details). MC13 expresses much more readily than Slo3 in the oocyte expression system and its basic gating properties are indistinguishable from Slo3 (**Suppl. Figs. 1 and 2**).

MC13 is insensitive to scorpion toxins. A hallmark of Slo1/BK-type channels is their sensitivity to the scorpion toxins, CTX and IbTX.[13,14] Whereas CTX sensitivity is shared with some voltage-dependent K^+ channels,[15] IbTX sensitivity appears unique to

Slo1 channels.[16] The ability of CTX and IbTX to block Slo1 and MC13 channels were compared in outside-out patches (**Fig. 1**). For Slo1 currents, the pipette solution bathing the cytosolic face of the patch contained 10 µM Ca^{2+} and currents were activated by voltage steps up to +160 mV. For MC13, currents were activated with a pipette solution containing pH 8.5 with voltage-steps up to +300 mV. Whereas nM concentrations of CTX effectively blocked Slo1 current (**Fig. 1A and C**), concentrations of CTX up to 100 nM were without effect on MC13 current (**Fig. 1B and D**). Similarly, IbTX produced a slow, concentration-dependent block of Slo1 current (**Fig. 1E**), while 100 nM IbTX was without effect on MC13 current (**Fig. 1F**). The family of Slo1 G/V curves with and without CTX was reasonably well fit with a state-independent blocking model with K_b = 6.1 ± 0.3 nM (**Fig. 1C**, red lines). This fit assumed zero voltage-dependence in the blocking equilibrium, since the duration of command steps was of short duration relative to the known durations of CTX unblocking relaxations.[8]

A segment of residues in the K^+ channel pore loop that connects the S5 outer helix and the pore helix that sits behind the K^+ channel selectivity filter is thought to contribute to the extracellular channel architecture, forming a so-called turret that surrounds the entry way to the permeation pathway. A recent study using IbTX binding has shown that this turret segment may contribute to CTX/IbTX binding in Slo1 channels.[12] Here we utilized Slo1/Slo3 chimeric constructs to identify parts of the P-loop that may underlie the differences in CTX sensitivity between Slo1 and Slo3. Replacement of the Slo1 P-loop with Slo3 sequence in construct MC6 resulted in complete insensitivity to 100 nM CTX (**Fig. 2A and B**). Replacement of the 2nd half of the Slo1 P-loop, including the selectivity filter and the pore helix, with Slo3 sequence in construct MC18 also resulted in insensitivity to 100 nM CTX (**Fig. 2C and D**). In contrast, replacement of the first half of the Slo1 P-loop (thought to contribute to the Slo1 turret) with Slo3 sequence in construct MC8 resulted in little or perhaps a modest reduction in CTX sensitivity (**Fig. 2E and F**). The effective K_b for CTX block of MC8 was 10.4 ± 0.3 nM, somewhat weaker than observed for Slo1. These results suggest that, although the 2nd half of the P-loop contains elements absolutely critical for CTX block, the first part of the P-loop may also contain elements that weakly influence CTX block. The persistence of CTX sensitivity in MC8 is somewhat surprising in that mutation Q267R in Slo1 abolishes IbTX binding.[12] R corresponds to the native homologous residue in Slo3. In addition, mutation of other Slo1 turret residues also influence IbTX binding. One explanation might be that turret residues may differentially influence IbTX binding and CTX block. For example, binding of the net +1 IbTX molecule may be more sensitive to the addition of charge at position 267 than the net +5 CTX molecule. Another possibility is that point mutations may disrupt a turret structure necessary for toxin binding, whereas replacing the entire turret segment in a chimeric construct may retain the necessary structure. Residue Y294 has also been previously implicated in IbTX binding.[12] Although the Slo1-Y294V construct was not totally insensitive to 100 nM CTX, the remaining block corresponds to an almost 100-fold reduction in CTX sensitivity (**Fig. 2G and H**). We attempted to
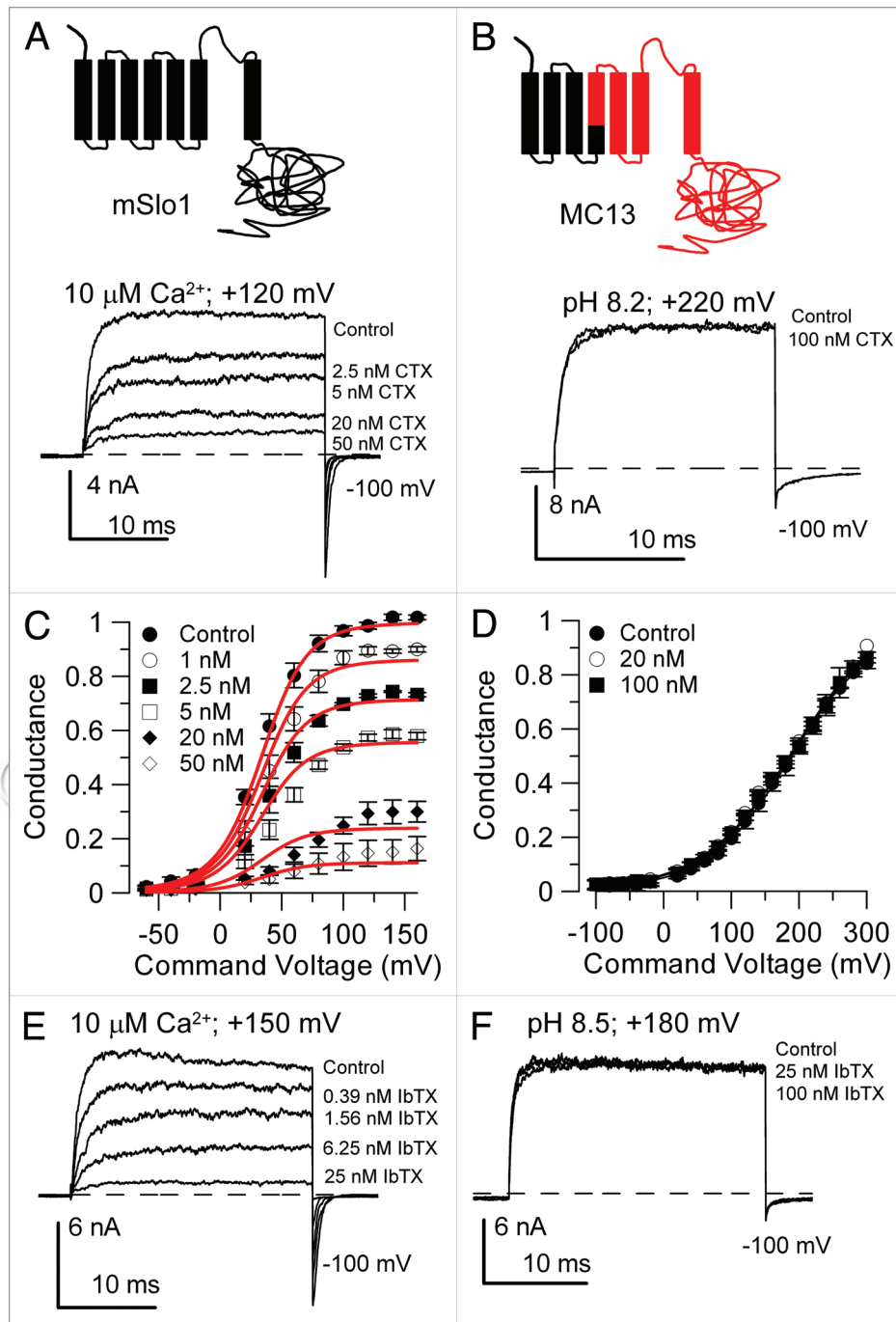
Figure 1. Slo3 is insensitive to block by CTX and IbTX. In (A), traces show block by cumulative application of CTX to an outside-out patch, with currents activated with 10 um Ca^{2+} at +120 mV. Cartoon on the top diagrams the Slo1 topology showing transmembrane segments and the cytosolic domain. In (B), 100 nM CTX is without effect on currents through the Slo3 surrogate construct, MC13. Currents were activated with a pipette saline of pH 8.2 with a depolarizing voltage step to +220 mV. The cartoon shows the MC13 topology with red elements originating from Slo3 and black elements from Slo1. See Methods for precise segment boundaries. In (C), Slo1 G/V curves are shown for different CTX concentrations. Red lines correspond to a fit of a state-independent blocking scheme (Scheme 2a) with $K_b = 6.1 \pm 0.3$ nM and no voltage-dependence during the time of each voltage-step. In (D), the effect of 20 and 100 nM CTX on MC13 G/V curves is shown. In (E), traces shown Slo1 currents during progressive increases in IbTX concentration to an outside-out patch with 10 μM pipette Ca^{2+} and activation steps to +150 mV. For comparison to other studies, fitting the fractional block of current by IbTX for values at +40 mV with a Hill equation yields a $K_d = 0.5 \pm 0.3$ nM ($n_H = 1$). In (F), MC13 currents are insensitive to application of 25 and 100 nM IbTX to an outside-out patch (activation with pipette pH of 8.5 at +180 mV).
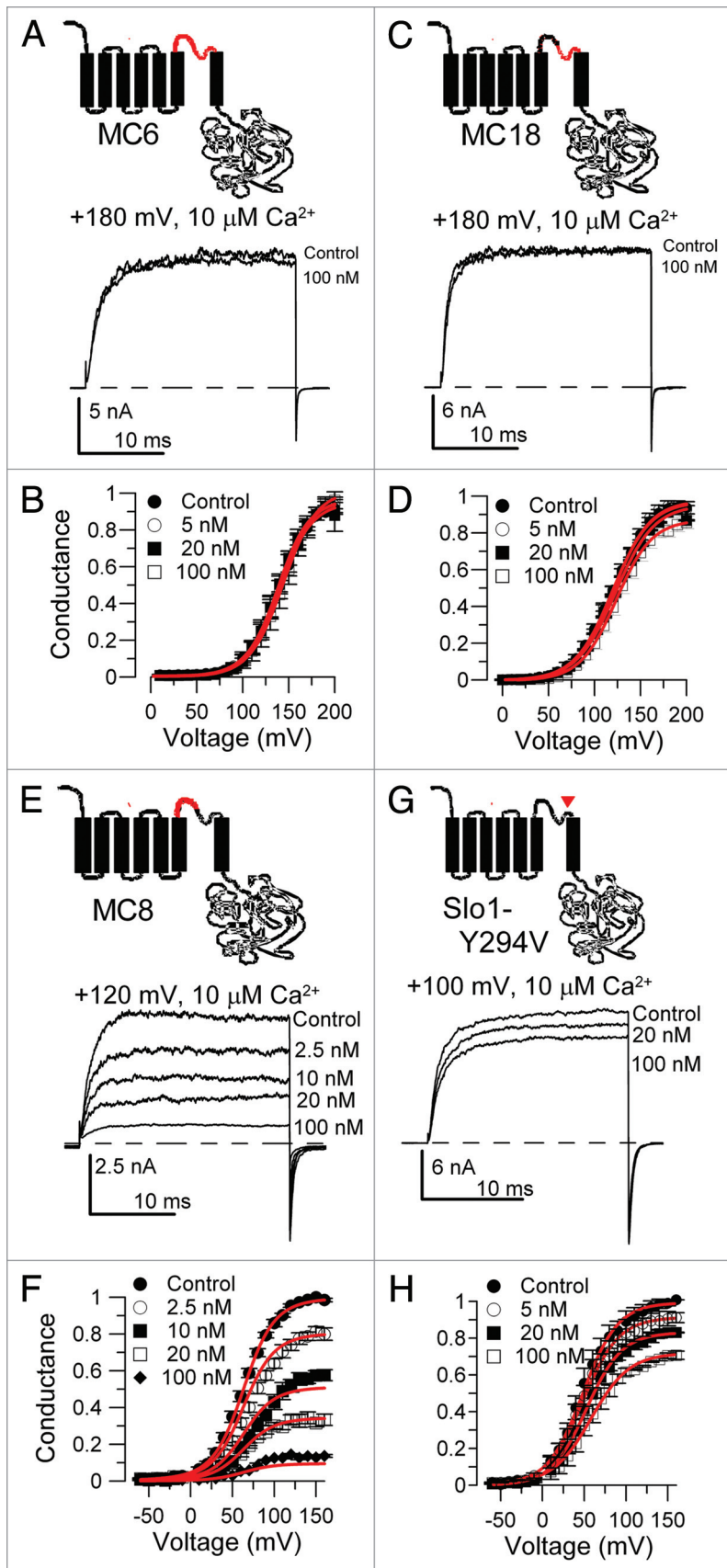
Figure 2. Slo1 CTX sensitivity arises primarily from Y294 with small contributions from other elements in the turret segment. In (A), traces show the lack of effect of 100 nM CTX on currents through construct MC6 (inset), in which the Slo1 P-loop is replaced with Slo3 sequence. In (B), G/V curves for MC6 activated with 10 μM Ca^{2+} are shown in the absence and presence of CTX. Red lines correspond to fits of a simple Boltzman function. In (C), traces show the lack of effect of 100 nM CTX on construct MC18, in which the 2nd half of the P-loop (selectivity filter and pore helix) were replaced with Slo3 sequence. In (D), G/V curves for the MC18 construct activated with 10 μM Ca^{2+} are shown. In (E), traces show that CTX readily blocks currents through construct MC8, in which the first half of the P-loop (primarily presumed turrent sequence) was replaced with Slo3 sequence. In (F), G/V curves for MC8 activated with 10 μM Ca^{2+} are shown at different CTX concentrations. Red lines correspond to the best fit of a state-independent blocking model (Scheme 2) with K_b = 10.4 ± 0.3 nM. In (G), traces show weak blocking effects of CTX on currents through Slo1-Y294V. In (H), effects of CTX on the Slo1-Y294V G/V curves are plotted for 10 μM Ca^{2+}.

engineer CTX sensitivity in MC13 with the MC13-V281Y mutation, but have been unable to obtain currents from this construct.

Block by both extracellular and cytosolic TEA differs between Slo1 and MC13. Another signature characteristic of Slo1/BK-type channels is blockade by extracellular TEA (TEA$_o$) at around 200–300 μM.[7,17] 250 μM TEA blocked Slo1 current about 50% at 0 mV with block being relieved at more positive potentials (**Fig. 3A**). The concentration-dependence of TEA effects on Slo1 G/V curves were somewhat better fit with a state-independent channel blocking model (**Fig. 3B**) than an open channel blocking model, with K_b = 173.9 ± 8.0 μM and zδ = 0.23 ± 0.02 e. These values are similar to estimates of TEA block (K_b ∼ 0.2 mM; zδ = 0.2 e) of open BK channels in bovine chromaffin cells,[7] but extend the earlier work to suggest that TEA affinity is identical in both closed and open BK channels. In contrast to the effects of TEA on Slo1 currents, TEA up to 10 mM had only minor effects on MC13. Similar to earlier work,[17,18] the Slo1-Y294V construct was relatively insensitive to TEA$_o$ being only slightly blocked at 10 mM, consistent with the slight block by 10 mM on MC13.

We also examined the sensitivity of Slo1 and MC13 to cytosolic application of TEA (TEA$_i$) in inside-out patches (**Fig. 4**). Block of Slo1 channels by TEA$_i$ (**Fig. 4A**) was well fit with an open channel block model[19] with an effective K_b = 49.0 ± 3.2 mM with zδ = 0.15 ± 0.02 e (**Fig. 4B**). Previous estimates for block of BK single channels either inserted in lipid bilayers or recorded from rat muscle with symmetrical K$^+$ solutions were 34.7 mM (zδ = 0.27 e)[20] and 60 mM (zδ = 0.26 e),[21] respectively, in general agreement with the present estimates. MC13 was substantially

more sensitive to block by TEA_i (**Fig. 4C**) with a concentration between 1 and 5 mM TEA producing more than 50% block of current over most activation voltages. Qualitatively, block of MC13 by TEA_i exhibited features quite distinct from block of Slo1 by TEA_i. In particular, the family of MC13 G/V's in the presence of TEA_i did not reveal any obvious increase in block with depolarization, in contrast to the properties of block of most K^+ channels by cytosolic quaternary ammonium blockers. However, it should be noted that there is a rapid voltage-dependent unblock on repolarization to -100 mV, since tail currents show only small reductions relative to the block observed at more positive potentials.

To fit the MC13 G/V curves we assumed that the fractional conductance at +300 mV with pH 8.5 was ~0.35 in accordance with previous estimates from Slo3.[5,6] Thus, over the entire activation range for Slo3, channels are activated at relatively low open probabilities. Irrespective of blocking model, estimates of the 0-voltage K_b for MC13 are complicated by the fact that the small current activation between 0 and +100 mV means that the amount of fractional block is not well-defined over that range. Thus, the estimates of 0-voltage values are highly dependent on the blocking model and voltage-dependence of block defined at the more positive potentials. We fit the G/V curves with both open channel and state-independent blocking models. The open-channel block model did a good job of accounting for fractional block over the entire voltage-range, but the best fit required a voltage-dependence in which block is relieved with depolarization (K_b = 0.11 ± 0.01 mM; zδ = -0.12 ± 0.01 e). This direction of voltage-dependence is not consistent with the expectation of the movement of the quaternary TEA molecule within the electric field. Furthermore, this direction of voltage-dependence also appears inconsistent with rapid unblock in the small tail currents. We also examined the ability of other blocking models to describe the G/V curves (**Suppl. Fig. 3**). A completely state-independent blocking model (Scheme 2a) resulted in a poorer fit to the G/V curves (**Table 1C**), while variants of Scheme 2 in which the closed and open state blocking affinity were allowed to differ did a somewhat better job of accounting for the block by TEA_i over all voltages, although again not as good as the open channel blocking scheme (**Table 1C**). No formulation of blocking models that included closed-channel block did as good a job as open-channel block at accounting for TEA block at low Po (**Suppl. Fig. 3**). Yet,
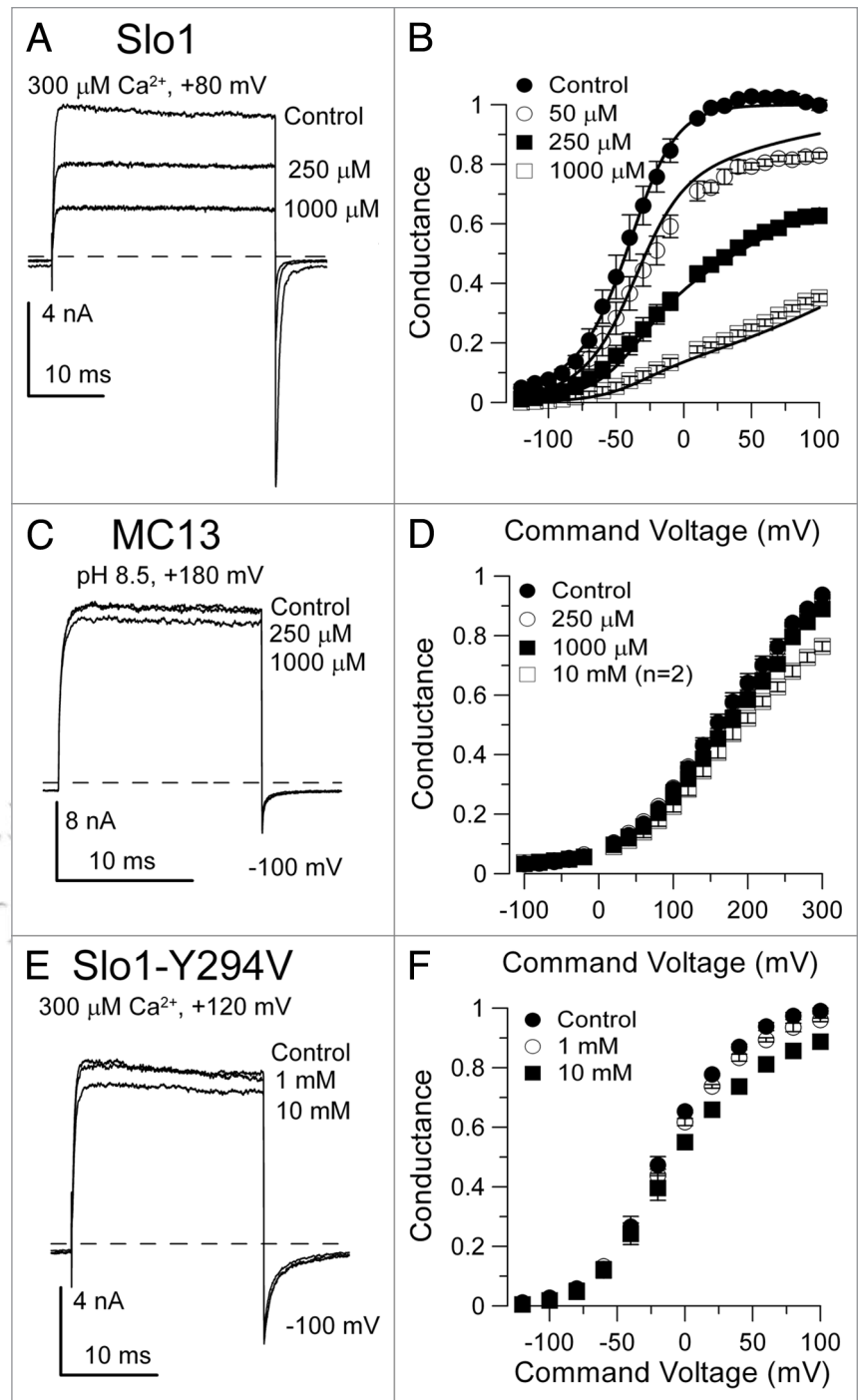
Figure 3. The Slo3 surrogate, MC13, is relatively insensitive to block by extracellular TEA in comparison to Slo1. In (A), application of TEA to outside-out patches inhibits Slo1 current. In (B), the effect of TEA on the Slo1 G/V curve generated with 300 M pipette Ca^{2+} is shown. The solid lines are the best fit of a state-independent blocking model (K_b = 173.9 ± 8.0 M; z = 0.23 ± 0.02 e). Block is relieved with depolarization. In (C), traces show weak blocking effects of extracellular TEA on MC13 currents in outside-out patches. In (D), extracellular TEA has minimal effect on MC13 G/V curves. In (E), mutation of Y294V in Slo1 abolishes most of the sensitivity of Slo1 to TEA. In (F), G/V curves summarize the lack of effect of TEA on the Slo1-Y294V construct.

Figure 4. MC13 is more sensitive than Slo1 to block by cytosolic TEA. In (A), traces show Slo1 current activated at +80 mV with 300 μM Ca^{2+} in the indicated concentrations of cytosolic TEA. In (B), G/V curves are shown for set of 4–5 patches with the lines showing the best fit of an op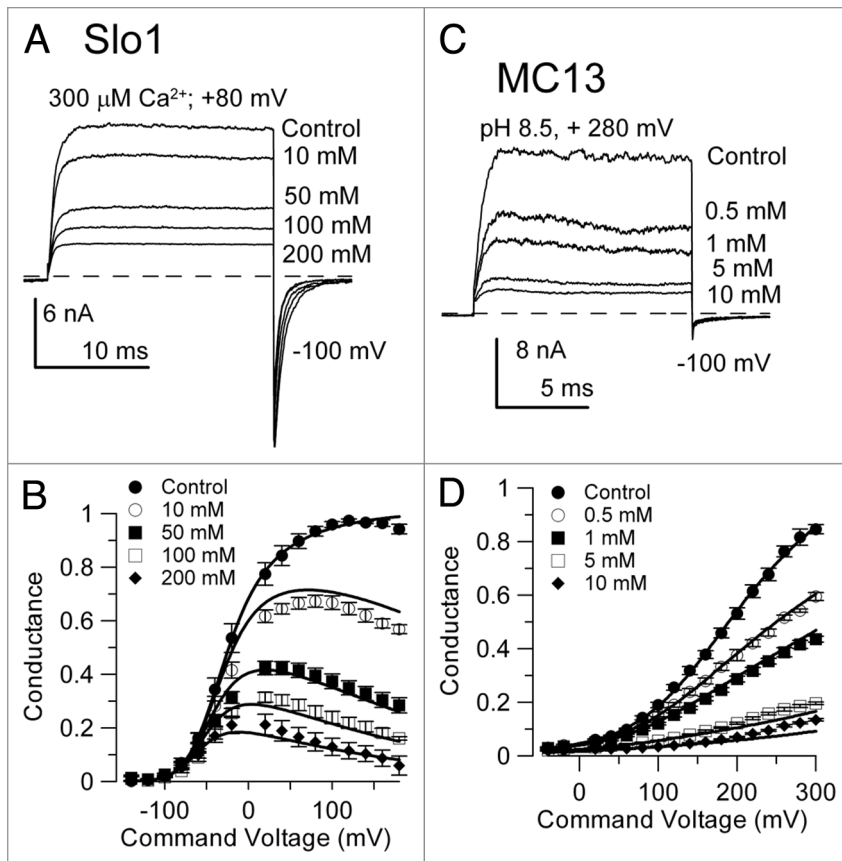en channel blocking model (K_b = 49.0 ± 3.2 μM; $z\delta$ = -0.15 ± 0.02 e). In (C), traces show MC13 currents activated with pH 8.5 at +280 mV at the indicated cytosolic TEA concentrations. In (D), G/V curves are shown for a set of 6 patches with the lines showing the best fit of an open channel block model (K_b = 0.11 ± 0.01 μM; $z\delta$ = 0.12 ± 0.01 e, with the maximal fractional conductance at +300 mV assumed to be 0.35,[5,6]). A state-independent model did not fit as well (see text and Suppl. Fig. 3).

the patches (**Fig. 5A and C**), and G-V curves were constructed from the steady-state current levels at each voltage (**Fig. 5B and D**).

For Slo1 G/V curves, blockade by extracellular 4-AP exhibits relief from block at more positive potentials (**Fig. 5B**). The direction of voltage-dependence is consistent with the idea that protonated 4-AP is the blocking species and, at more positive cytosolic potentials, is being driven from its blocking position on the extracellular side of the channel. In support of this idea, currents in the presence of 4-AP$_o$ also show time-dependent properties consistent with voltage-dependent movement of 4-AP in and out of blocking site at the extracellular side of the channel (**Fig. 5A**). Specifically, tail currents decay more rapidly in the presence of 4-AP$_o$ consistent with movement of an extracellular charged molecule into a blocking position within the electric field. Similarly, current activation by depolarizing steps in the presence of 4-AP$_o$ shows a slower activation time course qualitatively consistent with unblocking of channels that were blocked during the conditioning step to -120 mV. Extracellular 4-AP up to 100 mM produces little effect on MC13 currents.

The families of G-V curves obtained for Slo1 currents in the presence of different concentrations of extracellular 4-AP were reasonably well fit with a simple open-channel block model (**Fig. 5B**). This yielded a 0-voltage K_b for block of the open channel of 5.19 ± 0.41 mM with a voltage-dependence of z = 0.60 ± 0.03 e (see **Table 2A**). The state-independent blocking model did not provide a good fit to the G/V curves and attempts to achieve improved fits with a 2-site blocking model were unsuccessful. A surprising aspect of the block of Slo1 by extracellular 4-AP is its large voltage-dependence relative to block by extracellular TEA.

For MC13, the G/V curves suggest some slight block at high 4-AP$_o$ concentrations at positive potentials. This direction of voltage-dependence is in the opposite direction of that expected for a protonated blocker acting on the extracellular side of the channel. We suggest that this weak blocking action may reflect a very small accumulation of 4-AP on the intracellular side of the channel, consistent with the block by cytosolic 4-AP of MC13 described below. The small magnitude of this effect suggests that with an extracellular pH of 7.0 (0.0063% of 4-AP is uncharged) very little 4-AP accumulates on the cytosolic side of outside-out patches. Overall, based on the lack of effect of extracellular 4-AP on MC13, the affinities of Slo1 and Slo3 channels for 4-AP at 0 mV differ by at least 20-fold.

Effect of cytosolic application of 4-AP on BK, Slo3 and MC13 channels. In inside-out patches of Slo1 channels bathed with 300 μM Ca^{2+} at pH 8.5, 4-AP produced a rapid and reversible block over the range of 5–50 mM (**Fig. 6A**). Slo3 (**Fig. 6B**)

despite the better ability of open-channel block to describe the GV curves, the unusual voltage-dependence of that block seems at odds with the apparent rapid unblock in the tail currents. This uncertainty about the mechanism and voltage-dependence of block of MC13 by TEA$_i$ therefore precludes firm conclusions after block affinity. However, for comparison to block of Slo1 by TEA$_i$, 0.5–2 mM is probably a reasonable estimate of an upper limit for the 0-voltage affinity of TEA to its blocking site. Thus, Slo1 and Slo3 differ by about 25-fold in their sensitivity to cytosolic TEA near 0 mV.

Effects of extracellular 4-AP on Slo1 and MC13. 4-aminopyridine, a relatively non-selective K$^+$ channel blocker, has been reported to inhibit human sperm motility[10,11,22] and has also been shown to block some K$^+$ channels recorded in human sperm.[23] We first examined the ability of 4-AP to inhibit either Slo1 or MC13 current in outside-out patches. Slo1 currents were activated with 300 μM cytosolic Ca^{2+} at pH 8.5 (**Fig. 5A**), while MC13 currents were activated with pH 8.5 (**Fig. 5C**). For both constructs, mM concentrations of 4-AP at pH 7.0 were applied on the extracellular face of

Table 1A. Block of Slo1 by extracellular TEA (pipette saline: 300 μM Ca^{2+}, pH 8.5)

	OB (1a) 2 params	OB-CB (2a) 2 params	OB-CB (2') 4 params	OB-CB (2') $z_o = z_c = 0$ e
K_{bo} (μM)	131.6 ± 6.9	173.6 ± 8.0	175.7 ± 16.5	324.6 ± 17.7
z_o (e)	0.34 ± 0.02 e	0.23 ± 0.02 e	0.23 ± 0.04	0*
K_{bc} (μM)		173.6 ± 8.0	121.3 ± 37.5	52.2 ± 7.6
z_c (e)		0.23 ± 0.02 e	0*	0*
SSQ/pt	0.00135	0.00106	0.00966	0.001586
Norm SSQ	1.0	0.7852	0.7156	1.1745

Each column provides parameters for blocking constants from fits of a particular blocking scheme as described in the text; K_{bo} corresponds to affinity of blocker to open state, z_o, voltage-dependence of open state block, K_{bc} to affinity of blocker to closed state, and z_c, voltage-dependence of closed state block; SSQ/pt corresponds to sum of the squares for the fit of a given model only taking into account values obtained in the presence of bbTBA; Norm SSQ corresponds to SSQ/pt normalized to the open channel block model (1a); Negative values for z_o or z_c correspond to movement of charged particular in direction opposite the expected effect of the membrane field; *indicates parameter was fixed at the indicated value.

Table 1B. Block of Slo1 by cytosolic TEA (cytosolic saline: 300 μM Ca^{2+}, pH 8.5)

	OB (1a) 2 params	OB-CB (2a) 2 params	OB-CB (2') 4 params	OB-CB (2') $z_o = z_c = 0$ e
K_{bo} (mM)	48.96 ± 3.23	73.5 ± 4.5	78.6 ± 22.6	No convergence
z_o (e)	0.15 ± 0.02 e	0.22 ± 0.02 e	0.16 ± 0.20	
K_{bc} (mM)		73.5 ± 4.5	61.4 ± 34.8	
z_c (e)		0.22 ± 0.02 e	0.57 ± 0.32	
SSQ/pt	0.00082314	0.000766	0.000692	
Norm SSQ	1.0	0.9303	0.8402	

For Table legend, see Table 1A.

Table 1C. Block of MC13 by cytosolic TEA (cytosolic saline: 0 Ca^{2+}, pH 8.5)

	OB (1a) 2 params	OB (1a) $z_o = 0$ e	OB-CB (2a) 2 params	OB-CB (2') 4 params	OB-CB (2') $z_o = z_c = 0$ e
K_{bo} (mM)	0.11 ± 0.01	0.33 ± 0.01 e	2.01 ± 0.29	0.91 ± 2.77	0.56 ± 0.06
z_o (e)	-0.12 ± 0.01 e	0	0.05 ± 0.02 e	0*	0*
K_{bc} (mM)			2.01 ± 0.29	2.44 ± 0.64	2.36 ± 0.42
z_c (e)			0.05 ± 0.02 e	0.06 ± 0.20	0*
SSQ/pt	3.54E-05	0.000103	5.04E-05	4.7E-05	4.77E-05
Norm SSQ	1	2.912	1.424	1.328	1.346

For Table legend, see Table 1A.

and MC13 (**Fig. 6C**) currents activated at pH 8.5 were blocked to a similar extent by 4-AP, but at somewhat lower concentrations than block of Slo1 currents. Whereas reduction of the Slo1 conductance by 4-AP exhibited a weak voltage-dependence with stronger block at more positive potentials, any voltage-dependence in block of either Slo3 or MC13 was less obvious.

For each construct, the complete set G/V curves over all 4-AP concentrations were simultaneously fit with a simple-block scheme to obtain estimates of 0-voltage K_b and effective valence of block (**Table 2**). For cytosolic block of Slo1 by 4-AP, a single-site, open channel block model gave a poor fit of the G/V curves (**Table 2B**) with $K_b(0) = 24.2 ± 1.3$ mM with $z\delta = 0.03 ± 0.03$ e. The open channel block model did a better job of describing block of Slo3 and MC13 currents by intracellular 4-AP. For Slo3 currents, $K_b(0) = 2.1 ± 0.2$ mM with $z\delta = 0.02 ± 0.01$ e,

and for MC13, $K_b(0) = 2.5 ± 0.5$ mM with $z\delta = 0.02 ± 0.03$ e. Given that block of Slo3/MC13 is defined primarily by estimates of current amplitudes over the range of +100 to +300 mV, the estimate of $K_d(0)$ is basically an extrapolated value dependent on the magnitude of the estimate of $z\delta$. However, since block of Slo3 and MC13 by cytosolic 4-AP at pH 8.5 is only weakly voltage-dependent, the estimates of $K_b(0)$ give a reasonable estimate of the blocking effectiveness at 0 mV. Furthermore, it can also be seen from simple inspection that Slo1 currents are clearly less sensitive than Slo3/MC13 currents to cytosolic 4-AP. For each construct, we also evaluated whether models in which 4-AP blocks both open and closed states might better account for the G-V curves (**Table 2B–D**). For Slo1, the fit to the G-V curves was substantially improved by inclusion of block of both open and closed states ($K_b(0) = 30.7 ± 1.3$ mM, $z\delta = 0.10 ± 0.02$ e).
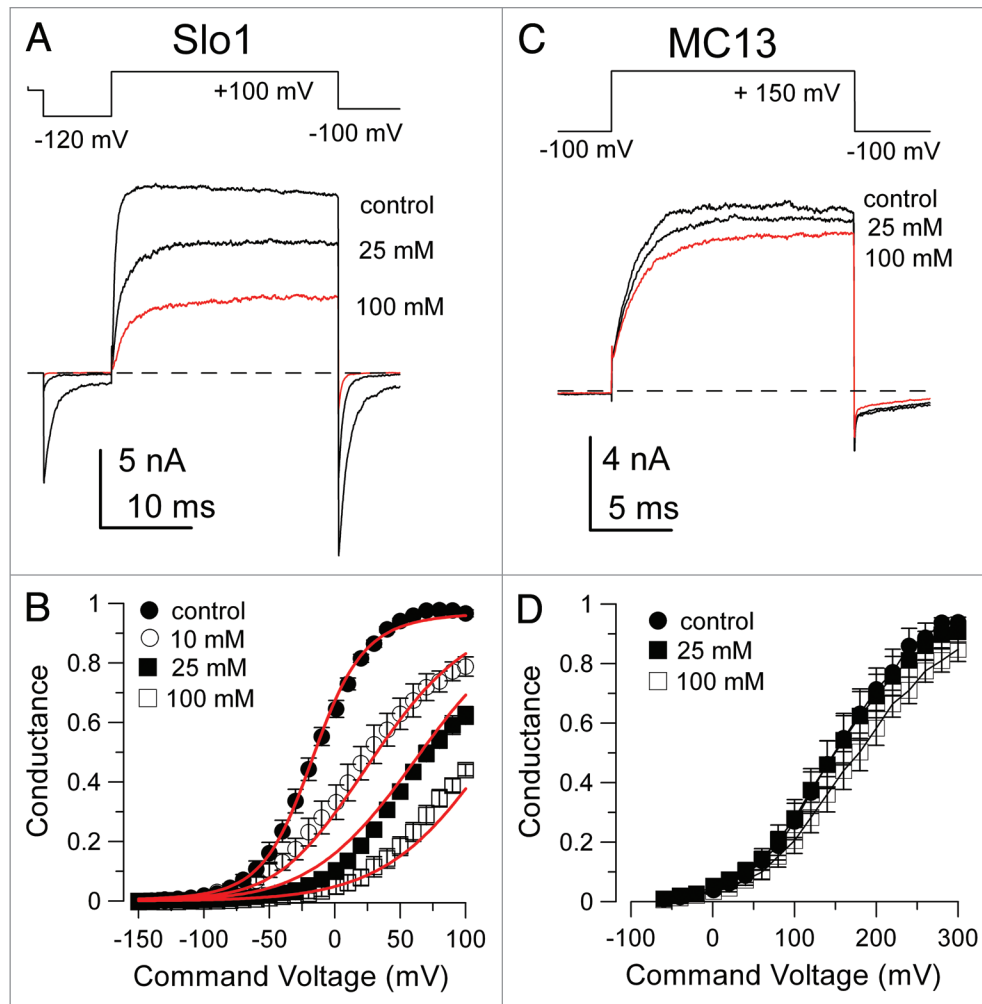
Figure 5. MC13 is relatively insensitive to block by extracellular 4-AP compared to block of Slo1. In (A), Slo1 currents were activated in outside-out patches by the indicated voltage-protocol with 300 μM Ca²⁺ (pH 8.5) inside the recording pipette. Application of 25 and 100 mM 4-AP resulted in substantial block of outward BK current. In the presence of 4-AP, activation at +100 mV is noticeably slowed, consistent with time-dependent unblock. In contrast, tail currents at -100 mV (red trace) in the presence of 4-AP decay more rapidly than in the absence of 4-AP and exhibit more block at the negative potentials. The pH of the extracellular solution was 7.0. In (B), G/V curves from traces such as those in (A) were generated from steady-state currents. Red lines are the best fit of the open channel block scheme with $K_b(0) = 5.19 \pm 0.41$ mM and $z\delta = 0.60 \pm 0.03$ e, consistent with a relief from block at more positive cytosolic voltages. In (C), MC13 currents were activated by the indicated voltage-protocol with the pipette solution at pH 8.5. 4-AP was much less effective in blocking MC13 than BK currents. In (D), G-V curves for MC13 currents were generated again revealing the relative lack of effect of extracellular 4-AP on MC13.

In contrast, for block by 4-AP of MC13 and Slo3, inclusion of closed channel block resulted in a poorer fit to the G/V curves (**Table 2C and D**).

We also compared the ability of cytosolic 4-AP to block Slo1 currents when applied at either pH 7.0 (**Fig. 7A**) or pH 8.5 (**Fig. 7B**) with 300 μM Ca²⁺. At pH 7.0, block of Slo1 channels by cytosolic 4-AP was somewhat weaker but exhibited a stronger voltage-dependence yielding a $K_b(0) = 58.4 \pm 2.3$ mM with $z\delta = 0.17 \pm 0.01$ e (**Fig. 7C**), when a simple blocking model was applied. At pH 8.5, the $K_b(0)$ estimated from a fit of the open channel block model was 24.9 ± 2.6 mM with $z\delta = 0.05 \pm 0.06$ e. The state-independent model (Scheme 2a) actually provided a better description of the G/V curves at 8.5, but not at 7.0. Consistent with these steady-state effects, examination of BK current traces showed that, at pH 7.0, repolarization to a negative

potential resulted in a very rapid and almost complete unblocking of all current blocked at a more positive potential (**Fig. 7A**). This is consistent with the clear voltage-dependence of 4-AP action at pH 7.0. In contrast, at pH 8.5, although currents at symmetrical potentials show some rapid unblocking upon repolarization, a much larger fraction of current remains blocked at pH 8.5 consistent with the overall weaker voltage-dependence of block (**Fig. 7B**).

Both the pH-dependent differences in voltage-dependence of block of steady-state conductance and the pH-dependence of fast and slow unblocking in tail currents suggest that there may be two independent effects of 4-AP, which differ based on pH. This may reflect the relative abundance of protonated and unprotonated species and is reminiscent of earlier work that has examined the pH dependence of 4-AP blocking effects on K⁺ currents

in rabbit Schwann cells.[24] We therefore evaluated the ability of a two site blocking model to account for the 4-AP block over all conditions. Since the relative concentrations of protonated and unprotonated 4-AP will differ substantially between pH 7.0 and pH 8.5 (see Methods), one possibility is that the fast block component reflects movement of protonated 4-AP in and out of a readily accessible blocking site, while the unprotonated form may block in a voltage-independent fashion that will therefore not reveal itself in kinetic relaxations. This idea is encapsulated in Scheme 3 (see Methods). Assuming a pKa = 9.2,[25] one can calculate the explicit concentrations of each species of 4-AP at a given pH, allowing sets of G/V curves obtained at both pH 7.0 and 8.5 to be fit simultaneously using three independent parameters, voltage, [4-AP], and pH. The resulting simultaneous fit using Eqn. 3 provides an excellent description of the basic features of the G-V curves both at pH 7.0 and at pH 8.5 (**Fig. 7E**), particularly the differences in voltage-dependence of block in the two cases and the greater block at potential negatives to 0 mV at pH 8.5. Values for the blocking parameters for un-protonated (u) and protonated (p) 4-AP were $K_{b(u)}$ = 9.1 ± 0.5 mM, $K_{b(p)}$ = 63.5 ± 3.8 mM and z_p = 0.19 ± 0.02 e. If allostery was permitted either between block and gating or between the two blocking constants,

no improvement in the fit was observed. We have not explored other variations of the two-site model. However, the ability of a basic two-site model to describe the steady-state results with only three free parameters coupled with the pH-dependence of the tail current behavior strongly supports the idea that protonated and nonprotonated 4-AP species block by distinct mechanisms. In contrast, single site models whether involving only open channel block, or both open and closed channel block, are not able to account easily for the pH-dependent changes observed both in steady-state block and tail current kinetics.

Block of Slo1 and MC13 by quinidine. A characteristic of quinidine block of many voltage-dependent K^{+} channels is that, although block can occur with either extracellular or cytosolic application, block is generally thought to arise from the action of the protonated form of quinidine acting on the cytosolic side of the channel.[26-28] However, there are examples where block of channels by quinidine has been reported to involve stabilization

Table 2A. Block of Slo1 by extracellular 4-AP (cytosolic saline: 300 μM Ca^{2+}, pH 8.5)

	OB (1a) 2 params	OB-CB (2a) 2 params	OB-CB (2') 4 params
K_{bo} (mM)	5.31 ± 0.41	7.91 ± 0.74	No convergence.
z_o (e)	0.61 ± 0.03 e	0.48 ± 0.04 e	
K_{bc} (mM)			
z_c (e)			
SSQ/pt	0.0012721	0.001652	
Norm SSQ	1	1.298273	

Each column provides parameters for blocking constants from fits of a particular blocking scheme as described in the text; K_{bo} corresponds to affinity of blocker to open state, z_o, voltage-dependence of open state block, K_{bc} to affinity of blocker to closed state, and z_c, voltage-dependence of closed state block; SSQ/pt corresponds to sum of the squares for the fit of a given model only taking into account values obtained in the presence of bbTBA; Norm SSQ corresponds to SSQ/pt normalized to the open channel block model (1a); Negative values for z_o or z_c correspond to movement of charged particular in direction opposite the expected effect of the membrane field; *indicates parameter was fixed at the indicated value.

Table 2B. Block of Slo1 by cytosolic 4-AP (cytosolic saline: 300 μM Ca^{2+}, pH 8.5)

	OB (1a) 2 params	OB-CB (2a) 2 params	OB-CB (2') 4 params
K_{bo} (mM)	24.2 ± 1.3	30.7 ± 1.3	33.5 ± 4.7
z_o (e)	0.03 ± 0.03 e	0.10 ± 0.02e e	0.12 ± 0.03
K_{bc} (mM)		30.7 ± 1.3	17.6 ± 12.5
z_c (e)		0.10 ± 0.02 e	0.33 ± 0.32
SSQ/pt	0.00913	0.000439	0.00424
Norm SSQ	1	0.48009	0.4644

For Table legend, see Table 2A.

Table 2C. Block of Slo3 by cytosolic 4-AP (cytosolic saline: 300 μM Ca^{2+}, pH 8.5)

	OB (1a) 2 params	OB (1a) 2 params	OB-CB (2a) 2 params
K_{bo} (mM)	2.14 ± 0.17	1.71 ± 0.03	16.91 ± 1.76
z_o (e)	0.04 ± 0.01	0*	0.16 ± 0.01
K_{bc} (mM)			
z_c (e)			
SSQ/pt	1.959E-05	2.38E-05	4E-05
Norm SSQ	1	1.21647	2.040132

For Table legend, see Table 2A.

Table 2D. Block of MC13 by cytosolic 4-AP (cytosolic saline: 300 μM Ca^{2+}, pH 8.5)

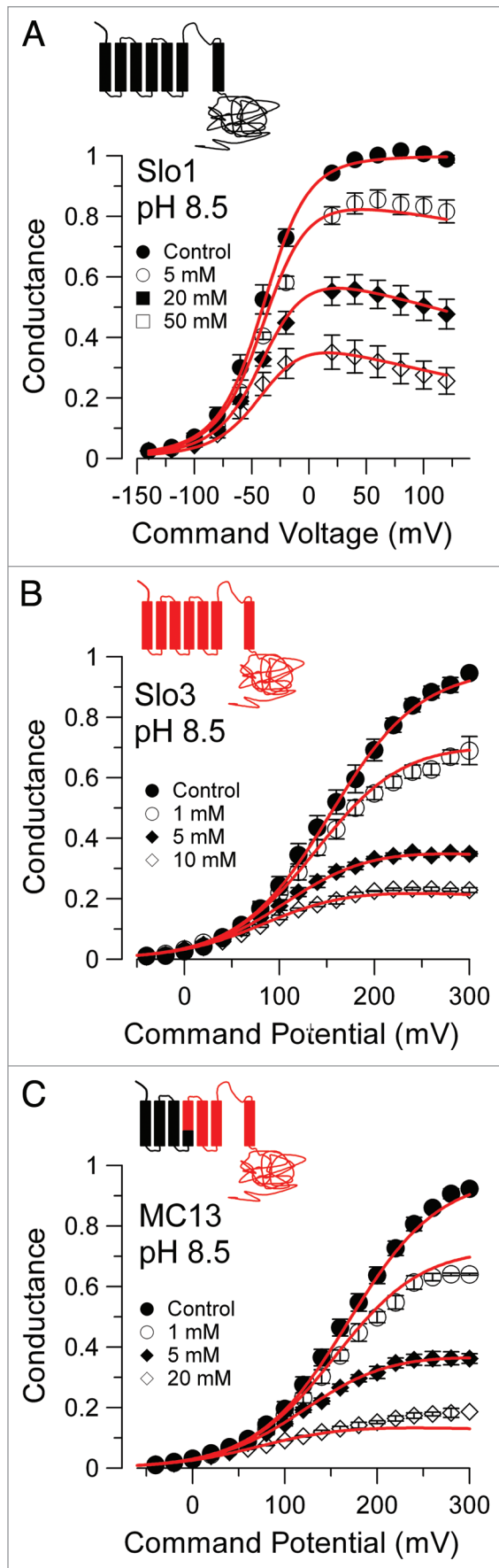|	OB (1a) 2 params	OB (1a) 2 params	OB-CB (2a) 2 params	OB-CB (2') 4 params
K_{bo} (mM)	2.47 ± 0.50	2.10 ± 0.08	20.74 ± 4.3	1.73 + 0.66
z_o (e)	0.02 ± 0.03	0*	0.17 ± 0.02	0*
K_{bc} (mM)				102.78 ± 409
z_c (e)				0.26 + 1.05
SSQ/pt	7.84E-05	7.839E-05	8.84E-05	8.45E-05
Norm SSQ	1	1.018	1.1273	1.0803

For Table legend, see Table 2A.

Figure 6. Cytosolic 4-AP blocks Slo3/MC13 more effectively than it blocks Slo1. In (A), G/V curves were generated for Slo1 currents activated with 300 μM Ca^{2+} (pH 8.5) in inside-out patches with various concentrations of 4-AP. Red lines are the best fit of Scheme 2a, the state-independent block model, with K_b = 30.7 ± 1.3 mM with zδ = 0.1 ± 0.02 e. In (B), G/V curves were generated for Slo3 currents activated with pH 8.5 and fit with Scheme 1, the open channel block model (K_b = 2.5 ± 0.5 mM with zδ = 0.02 ± 0.03 e. In (C), G/V curves were generated for MC13 currents activated in inside-out patches with pH 8.5 and fit with Scheme 1 (K_b = 2.1 ± 0.2 with zδ = 0.02 ± 0.01 e).

of closed states[29] or even actions of uncharged quinidine.[30] We have examined block of both Slo1 and MC13 by quinidine applied either on outside-out or inside-out patches. When applied to outside-out patches, the quinidine solution was at pH 7.0, for which quinidine is about 83% protonated (see Methods). For both inside-out and outside-out configurations, Slo1 channels were activated by 300 μM cytosolic Ca^{2+} at pH 8.5, while MC13 channels were activated with pH 8.5 with no Ca^{2+}.

Slo1 channels were blocked by mM concentrations of quinidine (**Fig. 8A**), with the resulting G/V curves revealing a weak voltage-dependence in the blocking effect (**Fig. 8B**). Overall, the G/V curves were well fit with Eqn. 1 based on an open channel block scheme with a $K_b(0)$ of 0.95 ± 0.02 mM and zδ = 0.047 ± 0.01 e (relief of block with depolarization), although other schemes also yielded adequate fits (**Table 3A**). Tail currents following repolarization in the presence of quinidine exhibited a rapid instantaneous unblock consistent with the direction of voltage-dependence observed in the G/V curves (**Fig. 8C**). This voltage-dependence of quinidine block in both the G/V curves and tail current kinetics is the opposite of that expected for a protonated blocker acting on the extracellular side of the channel. However, it is consistent with the idea that uncharged quinidine passes through the membrane with the protonated form then blocking from the cytoplasmic solution.[26] The ability of other blocking schemes to describe the G/V curves is summarized in **Table 3A**; in all cases, an increase in block both of closed and open channels was observed with depolarization (**Table 3A**).

Blockade of Slo1 currents by cytosolic quinidine (300 μM Ca^{2+} at pH 8.5) occurred at about 5-fold lower concentrations than for block by extracellular quinidine (**Fig. 8D and E**). The G/V curves exhibited somewhat more voltage-dependence of block than by extracellular quinidine and the fit of a simple block model yielded a $K_b(0)$ = 145.2 ± 2.8 μM with zδ = 0.17 ± 0.01 e. The direction of the voltage-dependence of the block was identical to that observed with extracellular application of quinidine, in both cases being qualitatively consistent with blockade by a positively charged moiety being favored by depolarization. This suggests that, in both cases, block may be occurring by a similar mechanism at a similar site.

To test the idea that block involves the protonated form of quinidine, block at pH 8.5 (**Fig. 8E**) was compared to block at pH 7.0 (**Fig. 8G**). At pH 7.0, the fit of the open channel block model to the G/V curves yielded $K_b(0)$ = 92.8 ± 9.8 μM with zδ = 0.11 ± 0.03 e. A change in pH from 8.5 to 7.0 (assuming a pK = 8.6,[26]) will result in an increase of protonated quinidine from
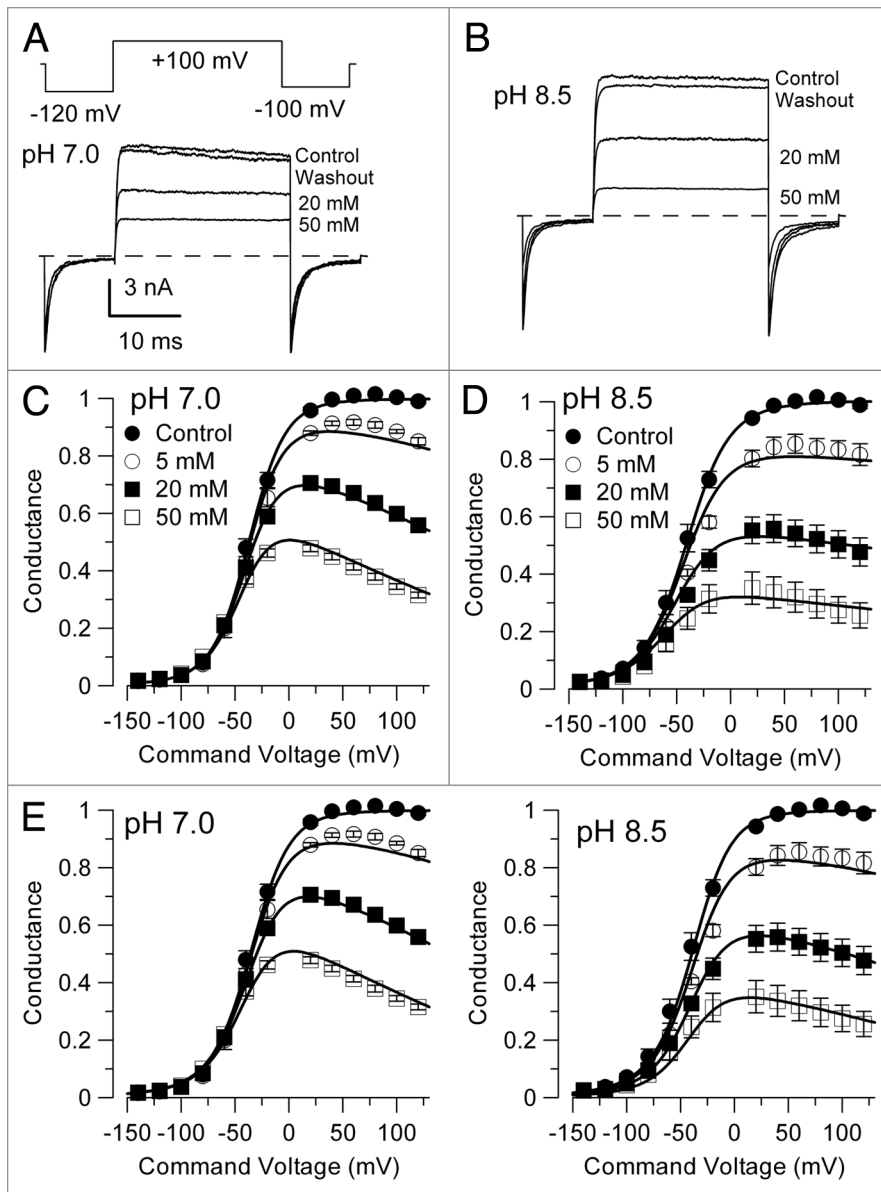
Figure 7. Comparison of block of BK currents by 4-AP at pH 7.0 and 8.5. In (A), currents activated with 300 μM Ca²⁺ at +100 mV by the indicated voltage protocol are compared for different 4-AP concentrations at pH 7.0. The trace for 50 mM 4-AP exhibits greater than 50% block at +100 mV with almost full and instantaneous recovery during the tail current at -100 mV. In (B), currents from the same patch as in (A) were activated as in (A) except at pH 8.5. The trace at 50 mM 4-AP shows strong block at +100 mV, with less complete recovery from block during the tail current in comparison to currents at pH 7.0. In (C and D), G-V curves at plotted for different concentrations of 4-AP either for pH 7.0 (C) or 8.5 (D). In (C), lines correspond to the best fit of Scheme 1a to all points for pH 7.0 yielding K_b = 58.3 ± 3.3 mM with $z\delta$ = 0.18 ± 0.02 e. In (D), similarly for pH 8.5, Scheme 1a yielded K_{bo} = 24.9 ± 2.6 mM with $z\delta$ = 0.05 ± 0.06 e. However, at pH 8.5, the state-independent Scheme 2a yielded a better fit than Scheme 1a, with K_{bo} = K_{bc} = 31.0 ± 2.7 mM with $z\delta$ = 0.11 ± 0.03 e, while for pH 7.0 Scheme 2a yielded a poorer fit than Scheme 1a. In (E), the G/V curves obtained at both pH 7.0 (left) and pH 8.5 (right) were fit simultaneously with Scheme 3, which assumes two independent 4-AP blocking sites, one for the uncharged non-protonated species defined by binding constant $K_{b(u)}$ and a voltage-dependent site sensitive to protonated 4-AP defined by binding constant $K_{b(p)}$. Best fit values for the three free parameters were $K_{b(u)}$ = 9.07 ± 0.46 mM, $K_{b(p)}$ = 63.5 ± 3.8 mM, and $z_{(p)}$ = 0.19 ± 0.02 e.

55.73% to 97.55%, or a 1.75 fold increase in protonated quinidine. This contrasts to an almost 10-fold decrease in non-protonated quinidine. The 1.75-fold increase in protonated quinidine is associated with an effective change in $K_b(0)$ of 1.56-fold (145.2 μM at pH 8.5 and 92.8 μM at pH 7.0). This general correspondence supports the idea that only protonated quinidine is responsible for block of Slo1 channels, whether applied intracellularly or extracellularly.

MC13 currents were blocked by substantially lower concentrations of extracellular quinidine than were Slo1 currents (**Fig. 9A**). Families of G/V curves reveal that block by quinidine is somewhat diminished at more positive activation potentials (**Fig. 9B**), with relatively strong block at potentials negative to +100 mV. However, one feature of the currents in the presence of quinidine is not easily reconcilable with the idea that depolarization is simply producing a relief of block. Specifically, traces of outward current in the presence of quinidine show some weak time-dependent increase in block at positive potentials (**Fig. 9A**). Thus, although the overall steady-state conductance exhibits a relief of block with depolarization, there appears to be some component of block that increases with depolarization. These properties of block by quinidine are also observed with cytosolic application of quinidine (**Fig. 9C and D**) although at about 5-fold lower concentrations.

Although the voltage-dependence of quinidine effects on the overall G/V curves is mechanistically at variance with the time-dependent block at positive potentials, we fit the G/V curves for outside-out application of quinidine with the various single site models of block. These results are summarized in **Table 3C**. No single model was clearly superior to any other. A simple open channel block mechanism (Eqn. 1; Scheme 1) fits the G/V curve data reasonably well with $K_b(0)$ = 1.25 ± 0.13 μM and $z\delta$ = 0.272 ± 0.01 e. However, other blocking models including block of both open and closed channels also describe the G/V curves reasonably well (**Table 3C**), with in all cases block relieved with depolarization. For example, for a state-independent blocking scheme (2a), $K_b(0)$ = 11.42 ± 1.44 μM with $z\delta$ = 0.13 ± 0.01 e. We also considered whether the unusual relief of
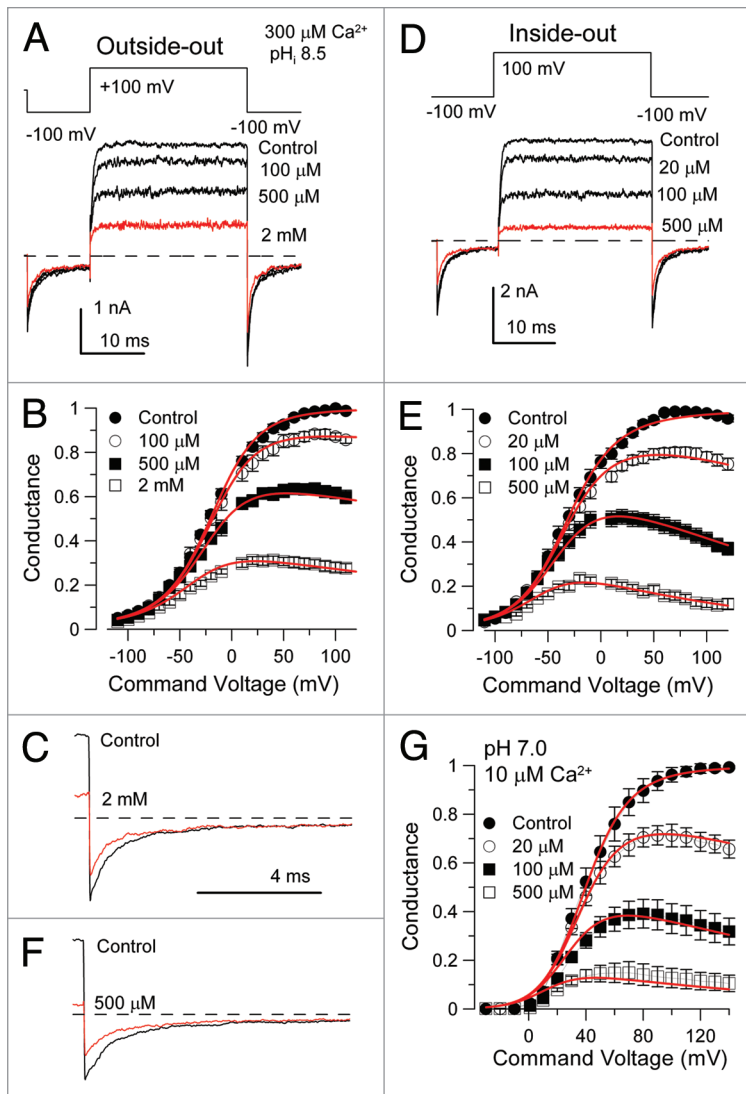
Figure 8. Block of Slo1 by extracellular or intracellular quinidine is increased by depolarization. In (A), the indicated voltage-protocol was used to elicit Slo1 currents activated with a cytosolic solution containing 300 μM Ca^{2+} at pH 8.5. Each trace was with a different concentration of extracellular quinidine (pH 7.0). In (B), G/V curves for Slo1 current activation in the presence and absence of quinidine exhibit increased block at more positive potentials. Red lines correspond to the fit of Eqn. 1 with $K_b(0) = 0.95 ± 0.02$ mM ($z\delta = 0.05 + 0.01$ e). In (C), tail currents following repolarization are shown on an expanded time base for the control trace and 2 mM quinidine trace (red) from (A), revealing rapid unblock upon repolariztion. In (D), traces show Slo1 currents in an inside-out patch activated with the indicated voltage-protocol with 300 μM cytosolic Ca^{2+} at pH 8.5 and the indicated quinidine concentrations. In (E), G/V curves for Slo1 currents with various quinidine concentrations are plotted along with a fit of Scheme 1, an open-channel block model, with $K_b(0) = 142.9 + 3.4$ μM ($z\delta = 0.18 ± 0.01$ e). In F, traces are tail currents from (D) for control and 500 μM quinidine solutions. The fractional reduction of peak instantaneous current at -100 mV is reduced relative to the fractional reduction of steady-state current at +100 mV. In (G), Slo1 G/V curves were generated from inside-out patches with 10 μM Ca^{2+} at pH 7.0 and the indicated quinidine concentrations with the best fit of Eqn. 1 yielding $K_b(0) = 92.8 ± 9.8$ μM with $z\delta = 0.11 ± 0.03$ e.

block with depolarization might arise from an ability of quinidine to stabilize closed states. To assess this, block of both open and closed states was assumed to be voltage-independent, resulting

in best fit values yielding $K_{bc} = 22.19 + 0.72$ μM with K_{bo} converging to large values. Although an adequate fit was obtained, the best fit did a poorer job of accounting for the apparent relief of block with depolarization than either Schemes 1a or 2 (**Table 3C**), although such a scheme worked well in fitting block of MC13 currents by cytosolic quinidine (**Table 3D**). We also examined the ability of the 2-site model embodied in Scheme 3 and described by Eqn. 3 to fit the G-V curves, hypothesizing that one site (with binding constant K_1 with voltage-dependence z_1) is identically accessible in both open and closed channels while a second site (binding constant K_2 with voltage-dependence z_2) is available when the channel is open and does not interact allosterically with the first site. We evaluated this with and without different constraints on z_1 and z_2, but no assumption resulted in a good description of the data. Although these considerations do not exclude the possibility that two sites of action are involved in quinidine effects, the analysis suggests that any contribution of an open-channel-like increase in block with depolarization to the overall G/V curves is minimal. This apparent discrepancy between the apparent voltage-dependence of block in the G/V curves and the time-dependent block in outward currents remains unexplained.

Blockade of MC13 by cytosolic quinidine also exhibited similar complexities with block occurring at ~4–5-fold lower concentrations (**Fig. 9C**) with a $K_b(0) = 0.46 ± 0.08$ μM with $z\delta = 0.27 ± 0.02$ e when fit with a simple open channel block model. With a state-independent block model (**Table 3D**), $K_b(0) = 1.97 ± 0.3$ μM with $z\delta = 0.13 ± 0.02$ e. Similar to block by extracellular quinidine, steady-state block in the GV curves appears to be relieved with depolarization. However, as with block by extracellular quinidine, this apparent relief of block with depolarization was at variance with a time-dependent increase in block observed in MC13 currents at some voltages and quinidine concentrations (**Fig. 9C**). This time-dependent block was also confirmed in patches in which currents from a larger number of repeated voltage steps were averaged. This blocking effect, irrespective of its small magnitude, would be expected to influence the G/V curves and complicate their interpretation within the context of any single model. We also examined the effects of quinidine on MC13 tail currents (**Fig. 9E**). MC13 tail currents typically exhibit a larger faster component that can be difficult to resolve followed by a smaller, slower component. Here we only note that block by quinidine persists during the tail current, at least qualitatively consistent with the observed strong block by quinidine at negative potentials in the GV curves. We also examined the ability of blocking models with various alternative assumptions to describe these G/V curves (**Table 3D**). The assumption of a voltage-dependence of block (0.1 e) comparable to quinidine block of Slo1 with block favored with depolarization completely failed to describe the G/V curves. However, when both open and closed channel block were assumed to be

voltage-independent, the quality of fit of the G/V curves was only somewhat reduced (**Table 3D**). This raises the possibility that the intrinsic binding equilibria are not voltage-dependent, but differential affinity of closed and open states for quinidine contributes to the apparent relief of block. The ability of different models to fit the MC13 G/V curves obtained with cytosolic application of quinidine are compared in **Supplementary Figure 4** (also **Table 3D**). Although, in the absence of a definitive mechanism of quinidine block, it is not possible to define a

specific binding constant for quinidine block of MC13, it is clear that MC13 is much more readily blocked by quinidine than the closely homologous Slo1 channel. In addition, the overall tendency of MC13 currents to exhibit relief from block by quinidine with depolarization may prove useful for defining pharmacological block of Slo3 currents in native cells. Irrespective of the complexities of the quinidine effects on MC13, MC13 is much more sensitive to quinidine than Slo1.

To examine the pH-dependence of the effects of quinidine on MC13, we compared block by cytosolic quinidine at both pH 8.5 (**Fig. 9D**) and at pH 8.2 (**Fig. 9F**). Larger changes in pH begin to reduce the MC13 current amplitudes, while a change from pH 8.5 to 8.2 is sufficient to increase protonated quinidine from 55.73% to 71.25% or a 1.28-fold increase. From the G-V curves at each pH, we defined an effective blocking affinity using Scheme 2a. At pH 8.5, $K_b(0) = 1.97 \pm 0.3$ μM, while, at pH 7.0, $K_b(0) = 0.98 \pm 0.03$ μM, with both fits constrained to same voltage-

Table 3A. Block of Slo1 by extracellular quinidine (cytosolic saline: 300 μM Ca^{2+}, pH 8.5)

	OB (1a) 2 params	OB-CB (2a) 2 params	OB-CB (2') 4 params
K_{bo} (μM)	950 ± 20	1490 ± 40	1510 ± 160
z_o (e)	0.05 ± 0.01	*0.17 ± 0.01	0.06 ± 0.08
K_{bc} (μM)			1200 ± 210
z_c (e)			0.66 ± 0.1
SSQ/pt	0.0001275	0.000179	6.25E-05
Norm SSQ	1	1.404837	0.490149

Each column provides parameters for blocking constants from fits of a particular blocking scheme as described in the text; K_{bo} corresponds to affinity of blocker to open state, z_o, voltage-dependence of open state block, K_{bc} to affinity of blocker to closed state, and z_c, voltage-dependence of closed state block; SSQ/pt corresponds to sum of the squares for the fit of a given model only taking into account values obtained in the presence of bbTBA; Norm SSQ corresponds to SSQ/pt normalized to the open channel block model (1a); Negative values for z_o or z_c correspond to movement of charged particular in direction opposite the expected effect of the membrane field; *indicates parameter was fixed at the indicated value.

Table 3B. Block of Slo1 by intracellular quinidine (cytosolic saline: 300 μM Ca^{2+}, pH 8.5)

	OB (1a) 2 params	OB-CB (2a) 2 params	OB-CB (2') 4 params
K_{bo} (μM)	142.9 ± 3.4	207.5 ± 7.4	No convergence
z_o (e)	0.18 ± 0.01	0.28 ± 0.02 e	
K_{bc} (mM)			
z_c (e)			
SSQ/pt	0.0001123	0.000363	
Norm SSQ	1	3.232637	

For Table legend, see Table 3A.

Table 3C. Block of MC13 by extracellular quinidine (cytosolic saline: pH 8.5)

	OB (1a) 2 params	OB-CB (2a) 2 params	OB-CB (2a) $z_c = z_o = 0.0$	OB-CB (2') 4 params	OB-CB (2') $z_c = z_o = 0$ e
K_{bo} (μM)	1.25 ± 0.13	11.42 ± 1.44	38.47 ± 1.7	1.29 ± 0.21	>>K_{bc}
z_o (e)	-0.27 ± 0.01 e	-0.13 ± 0.01 e	0.0*	-0.27 ± 0.02	0*
K_{bc} (μM)				101.8 ± 272.9	22.19 ± 0.72
z_c (e)				-0.55 ± 1.5	0*
SSQ/pt	0.00003216	4.88E-05	0.000144	3.15E-05	7.12E-05
Norm SSQ	1	1.517996	4.475	0.978224	2.2164

For Table legend, see Table 3A.

Table 3D. Block of MC13 by intracellular quinidine (cytosolic saline: pH 8.5)

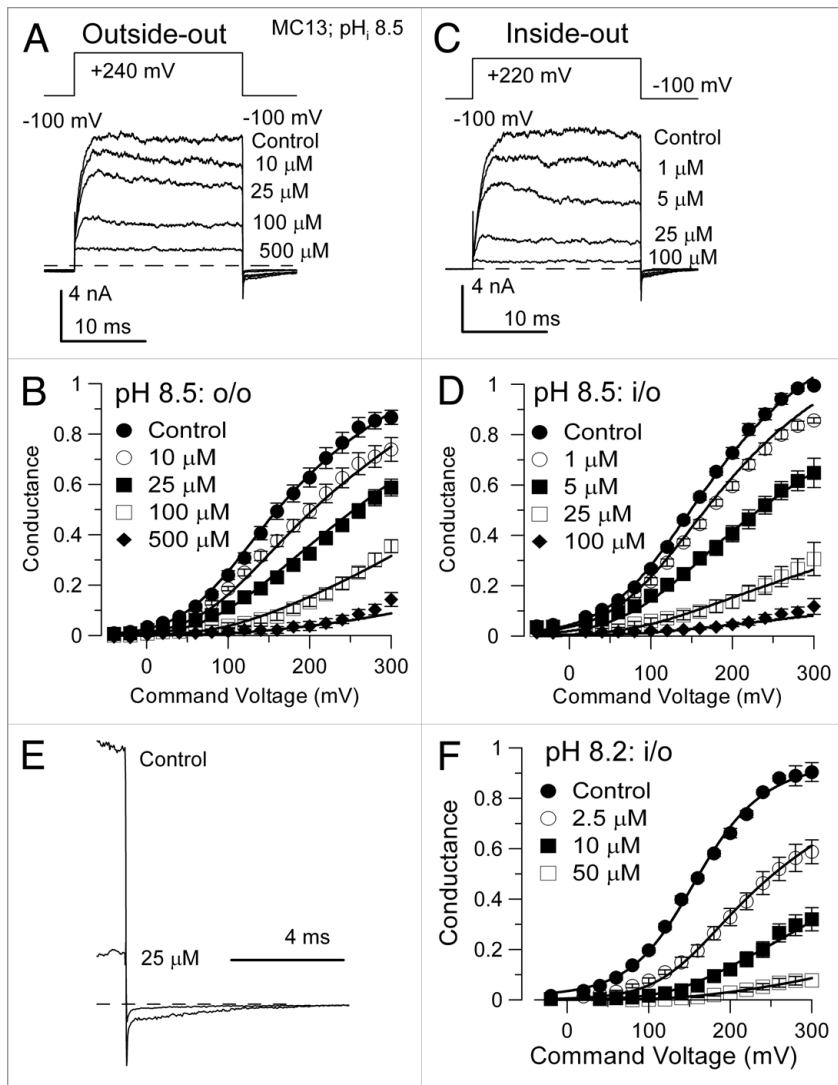|	OB (1a) 2 params	OB-CB (2a) 2 params	OB-CB (2a) $z_c = z_o = 0$	OB-CB (2') 4 params	OB-CB (2') $z_c = z_o = 0$ e
K_{bo} (μM)	0.23 ± 0.04	1.97 ± 0.3	6.34 ± 0.34	0.14 ± 0.06	>100000
z_o (e)	-0.26 ± 0.02	-0.13 ± 0.02 e	0.0*	-0.38 ± 0.10	0*
K_{bc} (μM)			6.34	42.3 ± 79.3	3.67 ± 0.16
z_c (e)			0.0*	-0.15 ± 0.38	0.0*
SSQ/pt	9.26E-05	8.16E-05	0.000158	8.38E-05	0.000102
Norm SSQ	1	0.929244	1.707333	0.904617	1.097485

For Table legend, see Table 3A.

Figure 9. Block of MC13 by either extracellular or intracellular quinidine shows a similar relief with depolarization. In (A), MC13 currents were activated in an outside-out patch with the indicated voltage-protocol with a pipette saline of pH 8.5. Quinidine (pH 7.0) was applied to the extracellular side of the patch. In (B), G/V curves for MC13 currents activated in various quinidine concentrations show relief of block at more positive potentials, particularly at higher quinidine concentrations. Lines correspond to a fit of Eqn. 2 (Scheme 2a; state-independent channel block) with $K_b = 11.42 \pm 1.44\ \mu M$ ($z\delta = 0.13 \pm 0.01\ e$ from the outside). In (C), traces show MC13 currents activated in an inside-out patch at pH 8.5 with the indicated quinidine concentrations. In (D), G/V curves from MC13 currents are plotted for the indicated quinidine concentrations. Lines show the best fit with Scheme 2a, a state-independent blocking model, with $K_b = 1.97 \pm 0.34\ \mu M$ with $z\delta = 0.13 \pm 0.02\ e$. In (E), traces are tail currents from (C) for control and 25 μM quinidine solutions, highlighting persistence of block with repolarization. In (F), G/V curves for MC13 currents obtained in inside-out patches at pH 8.2 with various quinidine concentrations are shown, with the best fit (Eqn. 2) yielding $K_b(0) = 0.98 \pm 0.03\ \mu M$, with $z\delta$ constrained to 0.13 e.

$K_b(0)$ is basically extrapolated from data at more positive voltages. However, the direction of the pH-dependence supports the idea that block of MC13 is mediated by the protonated form of quinidine and argues that the non-protonated form is unlikely to contribute to the blockade of MC13/Slo3 channels by quinidine.

The unusual relief of steady-state block by quinidine with depolarization, despite the fact that the blocking species appears to be protonated, raises question as to the origins of the voltage-dependence in the models we have fit to the data. As mentioned earlier, with models including both open and closed channel block, if the voltage-dependence of both closed and open channel block is set to 0 ($z_c = z_o = 0\ e$), reasonable fits to the G-V curves can be obtained (**Table 3C and D; Fig. S4**), without any intrinsic voltage-dependence in the binding equilibrium. Interestingly, in these cases, the affinity of $K_{bc}(0)$, the binding of quinidine to the closed channel, is markedly stronger than the affinity of binding to the open channel ($K_{bo}(0)$). Although the quality of the fit with such a model is not clearly better than the other models we have used, it points out that the apparent relief of block with depolarization may not reflect any intrinsic voltage-dependence of the drug binding equilibria, but rather a difference in affinity for quinidine between closed and open conformations.

Discussion

Here we have compared pharmacological properties of the pH-regulated Slo3 channel and its close homologue, the Slo1 or BK channel. For all blockers examined, clear differences between Slo3 and Slo1 channels were observed, despite the extensive amino acid identity through much of the pore-forming parts of these channels.[1] Here for each blocker, we consider the present results within the context of potential mechanisms of block and the potential utility of blockers for identification of Slo3 currents in native cells.

CTX, IbTX and TEA. Slo3/MC13 is unaffected by both CTX and IbTX, both of which block BK channels at low nM concentrations.[9,31,32] Our aim here was to attempt to identify those elements in Slo3 that may account for its resistance to CTX/IbTX block. In previous work, it has been shown that a number of residues both in the so-called turret region of the Slo1 channel and also following the selectivity filter can markedly reduce IbTX binding. This includes N268, L272 and E276 in the turret, and Y294 and K296 following the selectivity filter.[12] Here, we have focused on residue positions that differ between Slo1 and Slo3. Our results

dependence ($z\delta = 0.13\ e$). This corresponds to an approximately 2-fold change in effective $K_b(0)$ associated with an approximately 1.3 fold change in pH. Although this correspondence is not as close as observed for Slo1, the shifts in $K_b(0)$ may be difficult to define with accuracy because of uncertainties regarding blocking mechanism of MC13 channels by quinidine and the fact that

show that in the MC8 chimera, in which most of the Slo1 turret segment is replaced with Slo3 sequence, blockade of Slo1 currents by CTX is only slightly reduced. This argues that any determinants in the Slo1 turret that contribute to toxin binding are reasonably well-conserved in Slo3. Therefore, turret residues are not a major factor in contributing to the insensitivity of Slo3 to CTX. In contrast, mutation of Y294 to valine, its Slo3 counterpart, results in almost complete disruption of the ability of CTX to block the resulting current, in agreement with the importance of Y294 in supporting IbTX binding.[12] Although the present results show that the Y-to-V substitution in Slo3 may account for most of the Slo3 toxin resistance, it does not exclude the fact that other residues in Slo1, perhaps shared with Slo3, may also participate in toxin binding.

Concentrations of TEA$_o$ in excess of 50 mM are required to produce any reduction in Slo3/MC13 current, whereas Slo1 channels are typically half blocked around 200–400 μM.[7,17] Similar to the situation for CTX, the relatively weak blocking effect of extracellular TEA on Slo3 probably arises from the substitution of valine in Slo3 at the position corresponding to Y294 in the Slo1 sequence.[17] Consistent with earlier studies, we find the Slo1-Y294V construct is relatively insensitive to TEA.

Our results show that Slo3/MC13 is about 50–100 fold more sensitive than Slo1 to intracellular TEA. Blockade of Slo1 by TEA is thought to involve occupancy of the BK channel central cavity, although some features of block of Slo1/BK channels by quaternary ammonium blockers supports block of both closed and open channels.[33-35] For MC13/Slo3, block by cytosolic TEA can be fit adequately either with open channel or state-independent blocking models with weak voltage-dependence. An unusual aspect of the TEA$_i$ results is that, for the optimal fit of the open channel block scheme to GV curves derived from macroscopic currents, block is slightly relieved with depolarization. Typically such a result would argue against the open channel block possibility, since it is expected that block by the quaternary TEA should be favored by depolarization. Alternative models which included closed-channel block did a poorer job of accounting for TEA block at low Po. Unusual voltage-dependence of block might also arise because determinants of binding affinity within an open channel might undergo voltage-dependent changes, a possibility not typically addressed in evaluation of channel block. Although the discrepancy between the TEA steady-state voltage-dependence and the unblocking kinetics is curious, with the assumption that TEA is blocking in the MC13/Slo3 central cavity, we simply suggest that the TEA binding site exhibits little intrinsic voltage-dependence either as a result of movement within the field or as result of interaction with permeant ions. One difficulty in defining the voltage-dependence of block of MC13/Slo3 is that the weak intrinsic voltage-dependence of activation of MC13/Slo3 currents means that, even over a broad range of activation potentials, the MC13/Slo3 open probability increases only modestly. In contrast, for Slo1, block can be examined in part over a range of activation potentials where channels are almost maximally activated, thereby allowing easier visualization of the voltage-dependence of block. In future work, it will be interesting to examine the sensitivity of Slo3/MC13

channels to other quaternary blockers including bisquaternary species. Chimeric constructs containing the Slo3 pore but which activate at more negative voltages may be advantageous in such studies.

4-AP. Block of Slo1 channels by 4-AP$_o$ occurred at very high concentrations and the voltage-dependence and kinetic features of block were consistent with an extracellular site of action, while 4-AP$_o$ was without effect on MC13. In contrast, cytosolic application of 4-AP more effectively blocked MC13/Slo3 than Slo1, and in both cases block exhibited voltage-dependence consistent with a cytosolic site of action. It has previously been shown that extracellular 4-AP can permeate through membranes sufficiently to alter cytosolic pH, thereby indirectly resulting in reduction of Slo1 currents as the elevation of pH altered the buffering capacity of the EGTA-buffered solutions.[36] Here, the inability of extracellular 4-AP to block MC13/Slo3, while intracellular 4-AP readily blocked MC13/Slo3, argues that extracellular 4-AP at pH 7.0 does not permeate sufficiently through the membrane to produce a cytosolic concentration sufficient to block currents. This probably reflects the fact that at pH 7.0 and a pK of 9.2 only about 0.6% of the extracellular 4-AP will be uncharged. The magnitude of the slight blocking effect seen with 100 mM 4-AP$_o$ on MC13 would be consistent with a blocking effect of a total cytosolic 4-AP concentration on the order of 0.5 mM or less, which would be comparable to the extracellular concentration of the non-protonated form of 4-AP at 100 mM.

Block of Slo1 by intracellular 4-AP was of low affinity and exhibited a voltage-dependence characteristic of open channel block by a positively charged species. Furthermore, the pH-dependence of block of Slo1 by 4-AP supported the idea that the protonated and nonprotonated forms of 4-AP produce block in distinct ways. Specifically, with the assumption of a scheme in which protonated and unprotonated 4-AP act at distinct sites, we were able to fit simultaneously the G/V curves in the presence and absence of 4-AP at both pH 7.0 and 8.5. This model was also qualitatively consistent with differences in tail current behavior observed at each pH. Block of voltage-dependent K$^+$ currents in rabbit Schwann cells by 4-AP has also been proposed to involve distinct effects of both charged and uncharged species.[24]

Quinidine. Of the compounds examined, quinidine exhibited the strongest blocking effects on Slo3/MC13. Although the unknown aspects of the quinidine blocking mechanism preclude clear definition of blocking potency, block of MC13 channels may occur at ~100-fold lower concentrations than block of Slo1 currents at potentials near 0 mV. For both block of Slo1 and Slo3, quinidine exhibited some unusual features. In particular, whether applied to the extracellular or cytosolic face of a patch, block of MC13 currents was slightly reduced at stronger depolarizations, while block of Slo1 currents was weakly increased at more positive potentials. Yet, for block of either Slo1 or Slo3, quinidine was about 5-fold more effective when applied from the cytosolic face of the membrane.

Although there are complexities in quinidine action on MC13/Slo3 that we are unable to explain, quinidine block both for Slo1 and for Slo3/MC13 probably arises from protonated quinidine acting from the cytosolic face of the membrane. First,

the similarity of block of Slo1 by either quinidine$_o$ or quinidine$_i$, both in terms of magnitude and voltage-dependence, suggests that quinidine in both cases reaches the same blocking position. Second, block of MC13 also shows similarity in magnitude and voltage-dependence either with extracellular or cytosolic application of quinidine. Third, we showed that the blocking effect of cytosolic quinidine on both Slo1 and MC13 was pH-dependent with lower pH increasing the quinidine blocking effect. Thus, block is favored by increases in the fraction of protonated quinidine. For both Slo1 and MC13, there is an approximately 5-fold difference in blocking effectiveness between cytosolic and extracellular applications of quinidine. During extracellular application of quinidine, for block to be mediated by protonated quinidine on the cytosolic side of a patch, sufficient non-protonated quinidine must pass through the membrane to attain a concentration that is approximately 20% of the extracellular concentration, presumably resulting in an appreciable concentration of protonated quinidine in the pipette. In effect, with 100 μM total extracellular quinidine, the pipette concentration of quinidine would have to reach about 20–25 μM in a relatively short time, since the effects of quinidine are generally complete within tens of seconds.

Our analysis does not allow us to draw definite conclusions regarding the mechanism of quinidine block. Block by quinidine of MC13 shares with cytosolic TEA a tendency for block to be relieved with depolarization. This conflicts with the idea that a positively charged blocker reaches a blocking position from the cytosolic side. However, in both cases, models in which intrinsic binding affinity is voltage-independent can do an adequate job of fitting the data, when there is an affinity difference between block of open and closed channels. For quinidine, in particular, a much stronger affinity for binding to the closed state than the open state may play a role in producing the tendency for depolarization to relieve block. Although block of MC13 by cytosolic 4-AP appeared to accord better with open channel block, even in that case any voltage-dependence was very weak. To address more rigorously the issue of the voltage-dependence of block of the Slo3, it would be desirable to have a chimeric construct in which block can be studied over a full range of channel activation.

Are effects of 4-AP or quinidine on sperm motility related to effects on a Slo3 current? For both human and murine sperm, volume regulation is disrupted by 1–4 mM 4-AP, within the range of cytosolic 4-AP concentrations that produce half block of Slo3 current at pH 8.5. However, 4-AP, when applied extracellularly, exerts essentially no blocking effect on Slo3 currents. Thus, inhibition of Slo3 by 4-AP in a native cell would require that 4-AP accumulate to levels comparable to the extracellular concentrations. Although some accumulation is likely to occur, our results with extracellular application of 100 mM 4-AP suggest that the amount of 4-AP that accumulates on the cytosolic side of an outside-out patch bathed with 100 mM 4-AP at pH 7.0 is less than 1% or less than 1 mM. This argues that extracellular application of 1–4 mM 4-AP, the concentration effective in producing volume regulatory effects on sperm, would be unlikely to significantly block any native Slo3 current, unless extracellular pH was significantly higher. A secondary issue is

that accumulation of 4-AP in the cytosol will elevate cytosolic pH, thereby promoting Slo3 activation. Thus, any 4-AP induced elevation of cytosolic pH would act in opposition to the channel blocking effects of 4-AP.

Quinidine has also been observed to produce effects on sperm function, altering volume regulation, decreasing velocity, and affecting mucus penetration and migration.[10,11,22] These effects are not produced by TEA at 2.5–10 mM[10] so presumably involves a TEA-resistant channel. The quinidine sensitivity of the effects on sperm function remain incompletely defined, but effects have been reported at concentrations as low as 20 μM.[10] This is certainly within the range over which we observe that quinidine substantially inhibits Slo3 current when applied extracellularly. Quinidine is known to block a large number of different K$^+$ channels. For some, blockade occurs at much higher concentrations than reported here. For example, IRK1 is reported to be blocked with an EC$_{50}$ of 0.7 mM while ROMK1 is only moderately inhibited.[37] Block of IRK1 exhibits little voltage-dependence. However, for a number of voltage-dependent K$^+$ channels, quinidine effectively blocks currents at concentrations comparable to what we observe for block of Slo3, although blockade of voltage-dependent K$^+$ channels is in many such cases favored by depolarization.[27,28,38] With the unusual voltage-dependence of Slo3 block, i.e., that block is relieved by depolarization, Slo3 may be relatively more strongly blocked at potentials negative to 0 mV than many other K$^+$ channels. It should be noted that the native pH-dependent KSper K$^+$ channel is strongly block by 500 μM quinidine with activation at pH 7.5 and +100 mV.[4] It will be of interest to determine whether the block of the native KSper current by quinidine shares mechanistic features similar to quinidine block of Slo3.

In sum, the present results have defined distinct pharmacological differences between the closely related Slo1 and Slo3 K$^+$ channels, have provided quantitative information within the context of specific blocking models, have pointed out some potentially interesting questions regarding voltage-dependence and mechanism of Slo3 block, and, show that the quinidine sensitivity of Slo3 may account for some effects of quinidine on sperm function.

Materials and Methods

Oocyte removal and culture. The handling of stage IV *Xenopus laevis* oocytes for cRNA injection and expression was as previously described.[39,40] The Slo1,[40,41] and Slo3,[5,6] constructs were as previously described.

Constructs. The Slo1 and Slo3 constructs were identical to those employed in previous work from this laboratory.[41] The following chimeric constructs were constructed in which Slo1 sequence was replaced with homologous Slo3 sequence (numbering refers to residues in the native Slo1 or Slo3 sequence; homologous positions are displaced by 11 residues through much of the relevant region):

MC6-Slo1(1-258):Slo3(248-288):Slo1(300-1169);
MC8-Slo1(1-258):Slo3(248-268):Slo1(280-1169);
MC13-Slo1(1-181):Slo3(171-1121)
MC18-Slo1(1-279):Slo3(269-288):Slo1(300-1169);

The chimeric constructs were generated by over-lapping PCR, while the Slo1-Y294V construct was generated by site-directed mutagenesis with pfu DNA polymerase. The sequence fidelity of all constructs was verified by DNA sequencing at the Protein and Nucleic Acid Laboratory core facility of Washington University.

Properties of the MC13 construct. The MC13 construct was routinely used for most experiments as a surrogate for Slo3. This construct contains Slo1 sequence from residues 1–181 and expresses much more readily than Slo3. We find that the general properties of MC13 are indistinguishable from Slo3, including the dependence of gating on pH and voltage, the limiting Po at high pH and voltage, the shape of G/V curves, the weak voltage-dependence of activation at negative potentials, and basic properties of activation and deactivation time course (**Suppl. Figs. 1 and 2**). Regarding the pharmacological equivalence of MC13 and Slo3, we have compared cytosolic application of 4-AP, which was identical in both cases. Slo3 was also shown to be resistant to block by CTX and IbTX in a limited number of patches. For simplicity, when we refer to MC13/Slo3 in the Results and Discussion, we are general referring to MC13.

Electrophysiology. Current recordings utilized either inside-out or outside-out configurations[42] with an Axopatch 200 amplifier (Molecular Devices, Sunnyvale, CA). The Clampex program from the pClamp software package (Molecular Devices) was used to control voltage-command waveforms and acquire digitized currents. For recording of Slo3 current, pipettes were typically of less than 1 MΩ resistance,[5] while for other constructs resistances of ~1–2 MΩ were typically used. Pipettes were coated with Sylgard (Sylgard 184, Dow Chemical Corp.,) and then fire-polished. Gigaohm seals were formed in frog Ringer (in mM, 115 NaCl, 2.5 KCl, 1.8 CaCl$_2$, 10 HEPES, pH 7.4) and following excision, moved into flowing test solutions. Whether for outside-out or inside-out patches, the standard solution bathing the extracellular membrane face contained (in mM) 140 K-methanesulfonate, 20 KOH, 10 HEPES, 2 MgCl$_2$, pH 7.0 (titrated with methanesulfonic acid). For solutions bathing the cytoplasmic face of the patch membrane, the composition was (in mM) 140 K-methanesulfonate, 20 KOH, 10 HEPES with the pH adjusted to either 7.0 or 8.5 with HCl or KOH as necessary. In experiments with Slo1 channels, 300 μM Ca^{2+} was usually included in the activation solution, unless otherwise indicated. Solutions were exchanged at the pipette tip by a multi-barreled local application system.[43,44] Each tube was under separate valve control and solution flowed continuously from only one tube at a time. All experiments were at room temperature (~22–25°C). Salts for solution preparation were obtained from Sigma (St. Louis, MO).

Details of stimulation protocols are provided on the figures or in figure legends. In general, currents were activated with an activation protocol containing a set of sweeps with activation steps ranging from -100 up to either +200 (Slo1) or +300 (Slo3 or MC13). The interval between each sweep was typically 1 sec, with the holding potential between sweeps at 0 mV. A 10–20 ms prepulse to -120 mV was typically applied prior to the depolarizing test step. The duration of the depolarizing test step was set to ensure that currents were at steady-state during the test step.

Data analysis. Analysis of current recordings was accomplished either with Clampfit (Molecular Devices) or with programs written in this laboratory. In order to define the voltage-dependence of blocking equilibria, G/V curves were constructed from measurements of steady-state current. For families of G/V curves obtained within a patch, conductances were normalized to estimates of maximal conductance obtained in the absence of blocker.
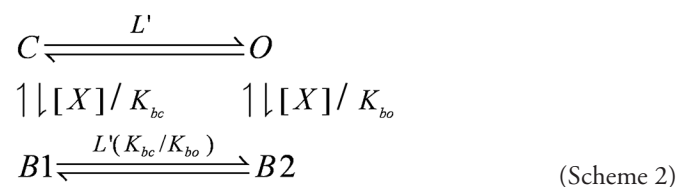
Although it is not the intent of this paper to rigorously test the validity of various blocking models in regards to any particular compound, blocking affinities can only be meaningfully defined within the context of knowledge of state-dependence of block. Towards this end, we utilized equations for fitting of specific mechanisms of block developed in a previous publication.[35]

$$ C \rightleftharpoons O \xrightarrow{[X]/K_{bo}} B \qquad \text{(Scheme 1)} $$
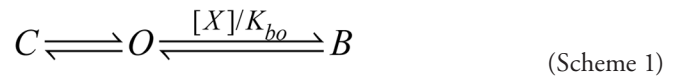
The general open channel block model is given in Scheme 1, where [X] represents the concentration of blocker binding with binding affinity K_{bo}. For Slo1 channels, activation is described by a multiple, tiered system of closed and open states involving four voltage-sensor transitions and four ligand binding steps.[45] As such, a full open channel block scheme contains additional tiers of blocked open states.[35] For a full activation scheme including open channel block, the blocking equilibrium is defined by:

$$ Po(Ca, V, [X]) = \cfrac{1}{1 + \cfrac{1}{L} \cfrac{(1 + J + K + JKE)^4}{(1 + JD + KC + JDKCE)^4} + \cfrac{[X]}{K_{bo} \exp^{\frac{-z_o FV}{RT}}}} $$

(Eqn. 1)

where $C_{term} = (1 + J + K + JKE)^4$ and $O_{term} = (1 + JD + KC + JDKCE)^4$. Similar equations have been utilized to describe Slo3 activation.[5,6] By incorporating explicit terms for activation into attempts to fit channel blocking models, these equations take into account the dependence of block on fractional channel activation. Since Slo1 channels typically open to maximal open probabilities in excess of 0.9, inclusion of explicit terms for channel activation are not so critical in defining blocking mechanisms for Slo1 channels. However, for Slo3 and MC13, for which channel activation only reaches values around 0.3–0.4 at pH 8.5 and +300 mV, assessment of blocking mechanism must take into account the conditions of channel activation.

$$ \begin{array}{ccc} C & \xrightleftharpoons{L'} & O \\ \big\updownarrow [X]/K_{bc} & & \big\updownarrow [X]/K_{bo} \\ B1 & \xrightleftharpoons{L'(K_{bc}/K_{bo})} & B2 \end{array} \qquad \text{(Scheme 2)} $$

A simplied form of a scheme that includes block of both open and closed channels in given in Scheme 2. Again, for a

full expansion of such a model to include the four voltage-sensor transitions and four ligand binding steps, the equilibrium predictions for a general model in which both open and closed channels can be blocked (Scheme 2) is the following:
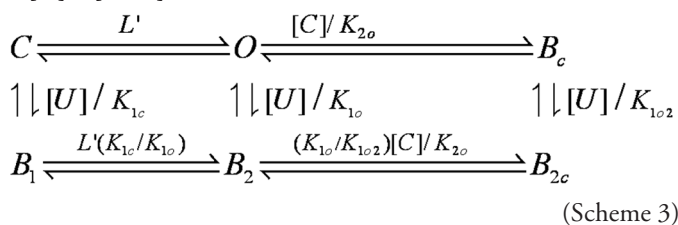
$$Po(Ca,V,[X]) = \cfrac{1}{1+\cfrac{1}{L}\cfrac{Cterm}{Oterm}+\cfrac{[X]}{K_{bo}\exp^{\frac{-z_o FV}{RT}}}+\cfrac{1}{L}\cfrac{Cterm}{Oterm}\cfrac{[X]}{K_{bc}\exp^{\frac{-z_c FV}{RT}}}}$$

(Eqn. 2)

For the case that $K_{bo}=K_{bc}$ and $z_o = z_c$, we term this Scheme 2a.

For Slo1, in which the maximal open probability approaches 1.0, the above equations can be simplified to the more typical equations which utilize a simple Boltzman to approximate the activation equilibrium. However, for Slo3 and MC13, in which the saturating conductance is not well-defined, we have felt it important to utilize equations that explicitly combine knowledge about fractional activation with channel block mechanisms.

In practice, here we have typically utilized only a single Ca^{2+} concentration or single pH to examine block. As such, the various terms for activation are not well-defined. The procedure we have followed is to first fit data obtained in the absence of blocker while constraining z_L, z_J and E to previously defined values 0.3 e, 0.58 e and 2.4 for Slo1,[45] and 0.04 e, 0.34 e and 1.4 for Slo3.[5] Since only a single ligand concentration was used, parameters for ligand equilibrium (K) and ligand coupling to channel activation (C) were also constrained either to values identical or close to previously published values. These constraints then allowed convergence on a set of estimates for L, J and D. For MC13 and Slo3, the G/V curves used for fitting were normalized such that fractional activation at +300 mV with pH 8.5 was assumed to be 0.35 based on previous work on Slo3 unitary current properties,[6] whereas for Slo1 the maximal conductance in G/V curves was assumed to approach 1.0. Once the activation parameters were defined, a complete set of G/V curves in the presence of blocker was then fit with equations 1 and 2 with all activation parameters constrained.

Two distinct blocking sites. We also tested the possibility that protonated and unprotonated 4-AP may bind to distinct sites, as previously suggested for block of K^+ currents in rabbit Schwann cells.[24] We hypothesize that the unprotonated form (U) may bind in a voltage-independent fashion to both closed and open states (states B_1 and B_2) with binding constants K_{1c} and K_{1o}, respectively, while the charged (C), protonated 4-AP binds only to the open channel (B_c) with binding constant (K_{2o}). We also define K_{1o2} as the binding affinity of the uncharged form, when the charged site is already occupied. This is summarized in Scheme 3, where [C] + [U] = [4-AP]:

$$
\begin{array}{ccccc}
C & \xrightleftharpoons{L'} & O & \xrightleftharpoons{[C]/K_{2o}} & B_c \\
\updownarrow {\scriptstyle [U]/K_{1c}} & & \updownarrow {\scriptstyle [U]/K_{1o}} & & \updownarrow {\scriptstyle [U]/K_{1o2}} \\
B_1 & \xrightleftharpoons{L'(K_{1c}/K_{1o})} & B_2 & \xrightleftharpoons{(K_{1o}/K_{1o2})[C]/K_{2o}} & B_{2c}
\end{array}
$$

(Scheme 3)

We define two allosteric coupling constants: $W = K_{1c}/K_{1o}$ and $Y = K_{1o}/K_{1o2}$. The total concentration of blocker [T] is given by [T] = [C] + [U]. At a given pH, [C] and [U] can be explicitly determined from the pKa for the blocking species. For 4-AP, the pKa is 9.2, so for a blocker concentration of [T] and a given [pH], [U] and [C] are both defined. From Scheme 3, the dependence of Po on voltage, [4-AP], and pH is:

$$Po(V,[X],pH) = \cfrac{1}{1+\cfrac{1}{L}\cfrac{Cterm}{Oterm}+\cfrac{1}{L}\cfrac{Cterm}{Oterm}A+B+D}$$

(Eqn. 3)

where

$$A = \cfrac{[U]}{W * K_{1o}\exp^{\frac{-z_{1c}FV}{RT}}},$$

$$B = \cfrac{[U]}{K_{1o}\exp^{\frac{-z_{1o}FV}{RT}}}, \text{ and}$$

$$D = \cfrac{[C]}{K_{2o}\exp^{\frac{-z_{2o}FV}{RT}}}+\cfrac{Y[C][U]}{K_{2o}K_{1o}\exp^{\frac{-z_{2o}FV}{RT}}\exp^{\frac{-z_o FV}{RT}}}$$

and [U] and [C] are explicitly defined by

$$[U] = [4AP]\cfrac{1}{1+\cfrac{10^{-pH}}{10^{-pKa}}} \text{ and } [C] = [4\text{-AP}] - [U].$$

For the situation that $W = 1$ ($K_{1c} = K_{1o}$), the unprotonated species binds with a single binding constant, K_{bu}. With $Y = 1$ (no interaction between binding of charged and uncharged species), the protonated species binds with a single binding constant, K_{bp} with voltage-dependence, z_c. Two other effects of protons might compromise use of the above approach. Specifically, protons are known to block Slo1 single channel currents[46] and shift Slo1 gating.[47] However, in the former case, voltage-steps to +120 mV with pH 7.0 are expected to have minimal effects on Slo1 single channel conductance. Concerning pH effects on Slo1 gating, we included a fixed pH-dependent shift in L for the change from pH 7.0 to 8.5 to reproduce the pH-induced G/V shift.

We note that the form of Eqn. 3 also provides a generic equation for a two site blocking mechanism, independent of pH, where one site is accessible in both open and closed channels, and one site is only reached when channels are open. In this case, terms A, B and D in the denominator of Eqn. 3 become:

$$A = \cfrac{[X]}{W * K_{1o}\exp^{\frac{-z_{1c}FV}{RT}}},$$

$$B = \cfrac{[X]}{K_{1o}\exp^{\frac{-z_{1o}FV}{RT}}}, \text{ and}$$

$$D = \cfrac{[X]}{K_{2o}\exp^{\frac{-z_{2o}FV}{RT}}}+\cfrac{Y[X][X]}{K_{2o}K_{1o}\exp^{\frac{-z_{2o}FV}{RT}}\exp^{\frac{-z_o FV}{RT}}}$$

When W = 1, binding to site one is identical both in open and closed channels. When Y = 1, binding to either site does not influence binding to the other site. However, in practice, the number of free parameters in this function can limit its utility.

For any given blocking model, we determined the sum of squares (SSQ) for the fit of a given model for points obtained in the presence of blocking drug. The SSQ per point was determined based on the number of points used in the fit. For comparisons among models, the SSQ/pt was normalized to that obtained for the open channel blocking model. Although the simultaneous fitting of families of G/V curves to models is a useful approach to assessing model adequacy, there are limitations. For example, a fit of a given model may result in a set of curves that closely parallel the actual data points, but be slightly shifted in apparent effective concentrations, resulting in appreciable contributions to the overall SSQ deviations. In contrast, another model may predict curves that do not parallel the data points as well, but by crossing the set of points at each concentration result in a lower overall SSQ deviation.

Control of ligand concentration during application of 4-AP or quinidine. In intact cells, membrane permeation by tertiary blockers can result in significant cytosolic accumulation. For whole-cell BK currents, interpretation of the blocking effects of extracellular application of 4-AP is complicated by the fact that passage of the tertiary amine, 4-AP, through the membrane can raise cytosolic pH.[36] When pH-sensitive cytosolic Ca²⁺ buffers are used to control Ca²⁺ concentration, the elevation in pH will decrease free Ca²⁺, thereby producing an apparent reduction in BK current amplitude unrelated to channel blockade. Similarly, any drug that produces changes in cytosolic pH would also influence Slo3 current activation, independent of blocking effects. We suspect that these potential problems are less likely to occur in excised patches where the medium bathing each face of the membrane is better controlled. However, there is the possibility that, in outside-out patches, drugs that permeate the membrane might alter the pH inside the recording pipette, thereby altering the concentration of the activating ligand. To minimize this concern, the following procedures were used. First, drugs applied to the extracellular side of outside-out patches were in solutions at pH 7.0, where the total concentration of uncharged, permeant species will be limited, particularly for 4-AP. Second, in outside-out patches, BK channels were activated with 300 μM cytosolic Ca²⁺ and no Ca²⁺ buffer. Any change in the pipette pH resulting from tertiary amine application will therefore not alter pipette [Ca²⁺]. Third, for Slo3 and MC13 in outside-out patches, currents were typically studied at a pipette pH of 8.5, a concentration producing near maximal current activation (**Supp. Figs. 1 and 2**). Thus, any local changes in pH within the pipette should have no effect on the activation equilibrium and the resulting G/V curves should therefore exclusively reflect blocking actions. For inside-out patches, currents were activated in a similar fashion, i.e., for BK channels with 300 μM Ca²⁺ at

pH 8.5 (unless otherwise indicated) or, for Slo3(MC13), by a cytosolic solution at pH 8.5. Thus, for both inside-out and outside-out patches, the effective concentration of activating ligand should not be influenced by the tertiary amine and any blocking effects observed in these studies should reflect exclusively effects on the channels.

Fractional voltage-dependence of block. Fractional voltage-dependence in any binding equilibrium is defined relative to the side of the membrane upon which a compound is acting. Thus, zδ = 0.2 for block from the cytosolic side is not the same position in the field as zδ = 0.2 for block from the extracellular side. Values for fractional voltage-dependence ideally reflect movement into the field from the side of entry. Here, in the case of quinidine, the blocking effects appear to arise following passage of unprotonated quinidine through the membrane to act on the cytosolic side of the channel. Thus, as used here, zδ for quinidine block is defined as movement relative to the cytosolic side of the channel. Block of MC13/Slo3 in some cases appears to involve an overall voltage-dependence that is inconsistent with simple movement of a protonated species in the membrane field. In such cases, the net zδ is negative in sign and, thus, the origins of this voltage-dependence can not be explained simply in terms of the standard Woodhull view of a positively charged species within the field of the membrane.[48]

Calculation of percent protonation for tertiary amines. Both 4-AP and quinidine are tertiary amines whose extent of protonation varies with pH. Based on pK, the percent, P, of the protonated form at a given pH was calculated from:

$$P = 100 - \frac{100}{1 + \frac{10^{-pH}}{10^{-pK}}}$$

For 4-AP, we assumed a pK of 9.2,[24] with the percent protonated 4-AP being 99.4% and 83.4% at pH 7.0 and 8.5, respectively. Quinidine contains two protonatable groups with one site having a pK near 4.2. pK values for the second site ranging from 8.0 to over 9.0 have been reported in the literature[49] and we use 8.6.[26] Protonated quinidine is 97.6%, 71.5% and 55.7% for solutions at pH 7.0, 8.2 and 8.5, respectively.

Note

Supplementary materials can be found at:
www.landesbioscience.com/supplement/TangCHAN4-1-Sup.pdf

References

1. Schreiber M, Wei A, Yuan A, Gaut J, Saito M, Salkoff L. Slo3, a novel pH-sensitive K+ channel from mammalian spermatocytes. J Biol Chem 1998; 273:3509-16.

2. de Lamirande E, Leclerc P, Gagnon C. Capacitation as a regulatory event that primes spermatozoa for the acrosome reaction and fertilization. Molecular Human Reproduction 1997; 3:175-94.

3. Navarro B, Kirichok Y, Chung JJ, Clapham DE. Ion channels that control fertility in mammalian spermatozoa. Int J Dev Biol 2008; 52:607-13.

4. Navarro B, Kirichok Y, Clapham DE. KSper, a pH-sensitive K+ current that controls sperm membrane potential. Proc Natl Acad Sci USA 2007; 104:7688-92.

5. Zhang X, Zeng X-H, Lingle CJ. Slo3 K+ channels: voltage and pH dependence of macroscopic currents. J Gen Physiol 2006; 128:317-36.

6. Zhang X, Zeng X-H, Xia X-M, Lingle CJ. pH-regulated Slo3 K+ channels: properties of unitary currents. J Gen Physiol 2006; 128:301-15.

7. Yellen G. Ionic permeation and blockade in Ca2+-activated K+ channels of bovine chromaffin cells. J Gen Physiol 1984; 84:157-86.

8. MacKinnon R, Miller C. Mechanism of charybdotoxin block of the high-conductance, Ca2+-activated K+ channel. J Gen Physiol 1988; 91:335-49.

9. Giangiacomo KM, Garcia ML, McManus OB. Mechanism of iberiotoxin block of the large-conductance calcium-activated potassium channel from bovine aortic smooth muscle. Biochem 1992; 31:6719-27.

10. Yeung CH, Cooper TG. Effects of the ion-channel blocker quinine on human sperm volume, kinematics and mucus penetration, and the involvement of potassium channels. Mol Hum Reprod 2001; 7:819-28.

11. Barfield JP, Yeung CH, Cooper TG. The effects of putative K+ channel blockers on volume regulation of murine spermatozoa. Biol Reprod 2005; 72:1275-81.

12. Giangiacomo KM, Becker J, Garsky C, Schmalhofer W, Garcia ML, Mullmann TJ. Novel alpha-KTx sites in the BK channel and comparative sequence analysis reveal distinguishing features of the BK and KV channel outer pore. Cell Biochem Biophys 2008; 52:47-58.

13. Miller C, Moczydlowski E, Latorre R, Phillips M. Charybdotoxin, a protein inhibitor of single Ca2+-activated K+ channels from mammalian skeletal muscle. Nature 1985; 313:316-8.

14. Galvez A, Gimenez-Gallego G, Reuben JP, Roy-Contancin L, Feigenbaum P, Kaczorowski GJ, et al. Purification and characterization of a unique, potent, peptidyl probe for the high conductance calcium-activated potassium channel from venom of the scorpion Buthus tamulus. J Biol Chem 1990; 265:11083-90.

15. Goldstein SA, Miller C. Mechanism of charybdotoxin block of a voltage-gated K+ channel. Biophys J 1993; 65:1613-9.

16. Candia S, Garcia ML, Latorre R. Mode of action of iberiotoxin, a potent blocker of the large conductance Ca2+-activated K+ channel. Biophys J 1992; 63:583-90.

17. Shen KZ, Lagrutta A, Davies NW, Standen NB, Adelman JP, North RA. Tetraethylammonium block of Slowpoke calcium-activated potassium channels expressed in Xenopus oocytes: evidence for tetrameric channel formation. Pflugers Arch 1994; 426:440-5.

18. Niu X, Magleby KL. Stepwise contribution of each subunit to the cooperative activation of BK channels by Ca2+. Proc Natl Acad Sci USA 2002; 99:11441-6.

19. Tang Q, Zeng X-H, Lingle CJ. Block of BK Channels by Quaternary Ammonium Compounds. J Gen Physiol 2009; 134:409-36.

20. Villarroel A, Alvarez O, Oberhauser A, Latorre R. Probing a Ca2+-activated K+ channel with quaternary ammonium ions. Pflugers Arch 1988; 413:118-26.

21. Blatz AL, Magleby KL. Ion conductance and selectivity of single calcium-activated potassium channels in cultured rat muscle. J Gen Physiol 1984; 84:1-23.

22. Barfield JP, Yeung CH, Cooper TG. Characterization of potassium channels involved in volume regulation of human spermatozoa. Mol Hum Reprod 2005; 11:891-7.

23. Gu Y, Kirkman-Brown JC, Korchev Y, Barratt CL, Publicover SJ. Multi-state, 4-aminopyridine-sensitive ion channels in human spermatozoa. Dev Biol 2004; 274:308-17.

24. Howe JR, Ritchie JM. On the active form of 4-aminopyridine: block of K+ currents in rabbit Schwann cells. J Physiol 1991; 433:183-205.

25. Albert A, Goldacre R, Phillips J. The Strength of Heterocyclic Bases. J Chem Soc 1948; 1948:2240-9.

26. Yeh JZ, Narahashi T. Mechanism of action of quinidine on squid axon membranes. J Pharmacol Exp Ther 1976; 196:62-70.

27. Snyders J, Knoth KM, Roberds SL, Tamkun MM. Time-, voltage- and state-dependent block by quinidine of a cloned human cardiac potassium channel. Mol Pharmacol 1992; 41:322-30.

28. Yeola SW, Rich TC, Uebele VN, Tamkun MM, Snyders DJ. Molecular analysis of a binding site for quinidine in a human cardiac delayed rectifier K+ channel. Role of S6 in antiarrhythmic drug binding. Circ Res 1996; 78:1105-14.

29. Yao JA, Trybulski EJ, Tseng GN. Quinidine preferentially blocks the slow delayed rectifier potassium channel in the rested state. J Pharmacol Exp Ther 1996; 279:856-64.

30. Voets T, Droogmans G, Nilius B. Potent block of volume-activated chloride currents in endothelial cells by the uncharged form of quinine and quinidine. Br J Pharmacol 1996; 118:1869-71.

31. Giangiacomo KM, Sugg EE, Garcia-Calvo M, Leonard RJ, McManus OB, Kaczorowski GJ, et al. Synthetic charybdotoxin-iberiotoxin chimeric peptides define toxin binding sites on calcium-activated and voltage-dependent potassium channels. Biochem 1993; 32:2363-70.

32. Giangiacomo KM, Garcia-Calvo M, Hans-Gunther K, Mullmann TJ, Garcia ML, McManus O. Functional reconstitution of the large-conductance, calcium-activated potassium channel purified from bovine aortic smooth muscle. Biochem 1995; 34:15849-62.

33. Li W, Aldrich RW. Unique inner pore properties of BK channels revealed by quaternary ammonium block. J Gen Physiol 2004; 124:43-57.

34. Wilkens CM, Aldrich RW. State-independent Block of BK Channels by an Intracellular Quaternary Ammonium. J Gen Physiol 2006; 128:347-64.

35. Tang Q, Lingle CJ. Closed channel block of BK potassium channels by bbTBA requires partial activation. J Gen Physiol 2009; 134:409-36.

36. Petkova-Kirova P, Gagov H, Krien U, Duridanova D, Noack T, Schubert R. 4-aminopyridine affects rat arterial smooth muscle BK(Ca) currents by changing intracellular pH. Br J Pharmacol 2000; 131:1643-50.

37. Doi T, Fakler B, Schultz JH, Ehmke H, Brandle U, Zenner HP, et al. Subunit-specific inhibition of inward-rectifier K+ channels by quinidine. FEBS Lett 1995; 375:193-6.

38. Fedida D. Gating charge and ionic currents associated with quinidine block of human Kv1.5 delayed rectifier channels. J Physiol 1997; 499:661-75.

39. Xia XM, Ding JP, Lingle CJ. Molecular basis for the inactivation of Ca2+- and voltage-dependent BK channels in adrenal chromaffin cells and rat insulinoma tumor cells. J Neurosci 1999; 19:5255-64.

40. Xia X-M, Zeng X-H, Lingle CJ. Multiple regulatory sites in large-conductance calcium-activated potassium channels. Nature 2002; 418:880-4.

41. Xia X-M, Zhang X, Lingle CJ. Ligand-dependent activation of Slo family channels is defined by interchangeable cytosolic domains. J Neurosci 2004; 24:5585-91.

42. Hamill OP, Marty A, Neher E, Sakmann B, Sigworth FJ. Improved patch-clamp techniques for high-resolution current recording from cells and cell-free membrane patches. Pflugers Archiv 1981; 391:85-100.

43. Herrington J, Solaro CR, Neely A, Lingle CJ. The suppression of Ca2+- and voltage-dependent outward K+ current during mAChR activation in rat adrenal chromaffin cells. J Physiol (Lond) 1995; 485:297-318.

44. Zeng X-H, Xia X-M, Lingle CJ. Gating properties conferred on BK channels by the β3b auxiliary subunit in the absence of its N- and C-termini. J Gen Physiol 2001; 117:607-27.

45. Horrigan F, Aldrich R. Coupling Between Voltage-Sensor Activation, Ca2+ Binding and Channel Opening in Large Conductance (BK) Potassium Channels. J Gen Physiol 2002; 120:267-305.

46. Brelidze TI, Magleby KL. Protons Block BK Channels by Competitive Inhibition with K+ and Contribute to the Limits of Unitary Currents at High Voltages. J Gen Physiol 2004; 123:305-19.

47. Hou S, Xu R, Heinemann SH, Hoshi T. Reciprocal regulation of the Ca2+ and H+ sensitivity in the SLO1 BK channel conferred by the RCK1 domain. Nat Struct Mol Biol 2008; 15:403-10.

48. Woodhull A. Ionic Blockade of Sodium Channels in Nerve. J Gen Physiol 1973; 61:687-708.

49. Grube S, Langguth P, Junginger HE, Kopp S, Midha KK, Shah VP, et al. Biowaiver monographs for immediate release solid oral dosage forms: quinidine sulfate. J Pharm Sci 2009; 98:2238-51.

50. Lingle CJ. Empirical considerations regarding the use of ensemble-variance analysis of macroscopic currents. J Neurosci Methods 2006; 158:121-32.